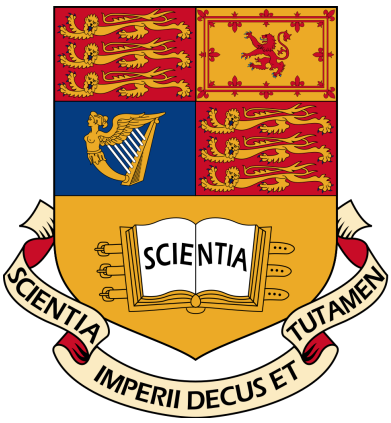

Imperial College London
Department of Physics

MSci Project Report

Black Hole Entropy in Causal Set Theory: Counting Molecules Over the Horizon

THEO-Dowker-1

by

00732522

Supervisor
Professor Fay Dowker
Assessor
Professor Kellogg Stelle

Word Count
9,987

May 2, 2017

Abstract

The source of black hole entropy within causal set theory is investigated. It is proposed that the number of causal set molecules crossing a black hole's event horizon corresponds to its entropy. Link molecules crossing the horizon are first counted in $2d$, by considering and developing previous analytical calculations. Computational analysis is then performed in $3d$ and finds that links cannot contribute to black hole entropy as they are not local to the horizon. So called z-triplet molecules are also investigated, both analytically in $2d$ and computationally in $3d$. These are shown to be local in both cases, and the number of them scales correctly with the area of the horizon, providing promise for the proposal.

Acknowledgements

Firstly I would like to thank my project partner. We had many fruitful and enjoyable meetings during which we tackled the problems outlined in this paper. It was great fun sharing my journey through black holes and discrete spacetime with 00735365.

Then, of course, comes our supervisor, Fay, with whom we met weekly. What started as 1 hour meetings eventually stretched beyond 2 hours as we discussed our work, deliberated over how to proceed and had general chats on topics ranging from physics to video games. Fay was always willing to impart her wisdom, and I thank her for providing the most intellectually stimulating part of my degree.

Finally I would like to thank Ian Jubb for showing interest in our work, providing quality advice and for his all-round friendliness.

Declaration

The project described in this report was carried out jointly by students 00735365 and 00732522.

The students jointly studied existing work on black hole thermodynamics and causal set theory and its application to black hole entropy.

The students jointly followed the work of Dou and Marr to understand different proposals for links as horizon molecules in $1+1D$. They jointly reproduced previous results, and added new insight by showing plain links cannot contribute to the entropy, an original result, and calculated corrections due to non-local contributions. Both students analysed z-triplets analytically in $1+1D$, and compared their results with those of Marr.

Both students worked on extending the analysis to higher dimensions. They examined the possibility of an analytical treatment, then designed an original computational method to count links. The structure of the algorithm was elaborated jointly by 00735365 and 00732522, with occasional guidance from graduate student Mr I. Jubb. Each student wrote their own code and produced independent but mutually consistent results. The analysis of x-links and xy-links in $1+1D$ is original. The investigation of links in $2+1D$, showing links cannot be horizon molecules in $2+1D$, is original and an important conclusion in terms of the interpretation of black hole entropy within CST.

The computational method for z-triplets is original and was implemented independently by each student, with consistent results. z-triplets had not been analysed in $2+1D$ before, so these are new results for the theory.

Nomenclature

Relativity/Causal Sets

nd	n dimensional spacetime.
$X+TD$	Spacetime with X spacelike dimensions and T timelike dimensions.
$J^+(x)$	The causal future of x.
$J^-(x)$	The causal past of x.
$\overline{\in}$	$x\overline{\in}A$ implies that x is the future-most element in A if A is a causal set, or the future-most element in a sprinkling on A if A is a spacetime region.
$\underline{\in}$	$x\underline{\in}A$ implies that x is the past-most element in A if A is a causal set, or the past-most element in a sprinkling on A if A is a spacetime region.
Timelike path	The path a massive particle follows in spacetime. All points on the path are causally related, i.e. timelike.
Null geodesic	The path a massless particle, e.g. photon, follows in spacetime.
Null hypersurface	A surface formed from all null geodesics emanating from a specific point.
$\prec$	$x \prec y$ implies x causally precedes y.
$\prec\!\!*$	$x \prec\!\!* y$ implies x and y are linked.
l_f	Discreteness length.
ρ	Discreteness (sprinkling) density, $\rho = l_f^{-n}$.

Mathematical Symbols

$:=$	Equals by definition.
$\in$	$x \in A$ implies x is an element of A.
$\forall$	For all.
$\cap$	$A \cap B$ equals all points/elements in both A and B (the intersection of A and B).

Other

Po$(k;\lambda)$	The Poisson distribution. The probability of k events occurring given a mean number of events λ.

Physical Constants

G	Newton's gravitational constant.
c	Speed of light.
$\hbar$	Reduced Planck's constant.

Natural units $G = c = \hbar = 1$ will be used unless otherwise specified.

Contents

Chapter 1

Introduction

Einstein's general theory of relativity (GR) [1] is a classical theory of gravity that has made innumerable contributions to black hole physics over the past century [2]. Notably, work by Stephen Hawking and Jacob Bekenstein in the 1970s showed that a black hole has an entropy that is directly related to its event horizon [3, 4], however the physical source of this entropy is not understood. In thermodynamics, the entropy of a system is related to the disorder of molecules within it, but if a black hole is truly black what could the analogue of these molecules be? The answer is thought to arise from quantum mechanics and thus a quantum theory of gravity is eagerly sought.

There is currently no scientific consensus on the correct quantum theory of gravity, however one particularly promising approach is causal set theory (CST) [5,6]. Pioneered by Rafael Sorkin in the late 1970s, one of CST's key hypotheses is that spacetime is fundamentally discrete. Just like matter, spacetime is thought to be made of atoms, which in turn form molecules. This led Sorkin to propose that black hole entropy is related to the number of spacetime molecules in the vicinity of the event horizon, the *horizon molecules* [7].

The objective of this work is to count different types of spacetime molecule, lying in the vicinity of the event horizon, to determine the entropy they produce. This will be compared with a well established theoretical formula for the entropy to critically test Sorkin's proposal. This work will start by analysing the simplest type of molecule in $1+1D$, before then testing different molecules and investigating higher dimensions, with the ultimate aim of finding viable horizon molecules.

Although we currently lack the experimental capabilities of measuring an astrophysical black hole's entropy, condensed matter physicists are able to create black-hole-like systems in their laboratories [8–13]. For example, using Bose-Einstein condensates, one can make a sonic black hole within which phonons cannot escape. This enables experimental study of the physical mechanisms behind black hole entropy, hence obtaining a theoretical understanding is a timely endeavour.

The exact structure of this report is as follows. Chapter 2 begins by introducing black holes and summarising how they arise in GR. The notion of black hole entropy is introduced, together with a heuristic understanding of its relation to both the event horizon and spacetime. Chapter 3 then introduces causal set theory, explaining its motivations and describing its mathematical structure. Moreover, spacetime molecules are introduced, together with an analytical method of counting them. Chapter 4 presents the proposal made by Sorkin, that the entropy of a black hole is (approximately) equal to the number of spacetime molecules lying across its event horizon. This is critically discussed, with the establishment of mathematical criteria that the number of molecules must satisfy for the proposal to be viable. Following the work of Dou [14, 15] and Marr [16], whilst adding mathematical detail, chapter 5 provides an analytical test of the proposal for a class of molecules known as links, in $1+1D$. It is found that the most simple

type of link does not satisfy the proposal, however alternative constrained links are found that do. In order to test the proposal in higher dimensions a computational approach is required due to analytical intractability. Chapter 6 describes an original algorithm that can be used to count link molecules in arbitrary many dimensions, detailing both its efficient features and inaccuracies. This algorithm is then implemented and tested against the previously obtained $1 + 1D$ results, showing good agreement. It is then used to show that all types of link do not satisfy the criteria of the proposal in $2 + 1D$, thus motivating the search for a different molecule that does satisfy the criteria. Chapter 7 introduces triplet molecules, notably so called z-triplets. Following the analytical work of Marr [16], these are shown to satisfy the criteria of the proposal in $1 + 1D$. Computational analysis of z-triplets is then performed, showing them to be consistent with the proposal in $2 + 1D$, providing great promise that z-triplets could be molecules that contribute to black hole entropy. Finally, chapter 9 summarises the conclusions of this project and identifies areas for future research.

Chapter 2

Black Holes

Black holes arise from the Schwarzschild solution to the Einstein field equations of GR. This chapter outlines the Schwarzschild solution, as well as black hole thermodynamics.

2.1 The Schwarzschild Solution

The Schwarzschild solution of GR describes the spacetime geometry outside a sphere of mass M [17]. It is spherically symmetric and displays interesting behaviour at a radial distance $r = 2M =: R_S$ from the mass, where R_S is known as the Schwarzschild radius. A plot of the trajectories of photons within this spacetime is shown in figure 2.1. All ingoing photons pass straight through the line $r = R_S$, suggesting nothing physical happens there. However, all photons within the $r < R_S$ region are directed towards $r = 0$, therefore any matter within $r < R_S$ is trapped there forever. This region is known as a black hole and the boundary $r = R_S$ is the event horizon, as no event inside the horizon can affect an event outside [18]. The event horizon is not a physical entity, just a mathematical point of no return.

Also, the Schwarzschild solution contains a singularity in the curvature of spacetime at $r = 0$. This is the 'centre' of a black hole, where all matter within the horizon will inevitably reach [19].

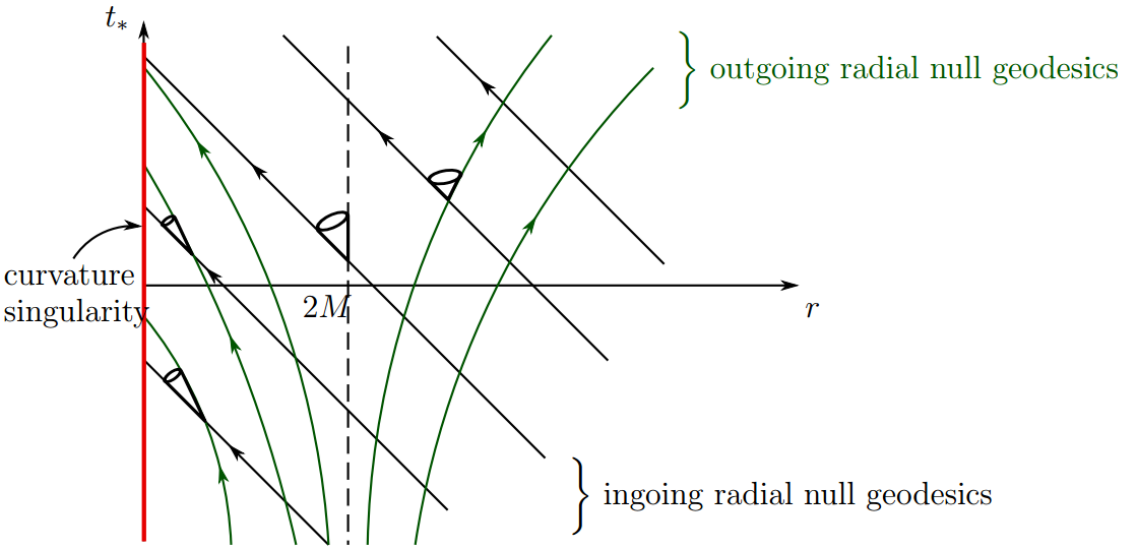

Figure 2.1: A spacetime diagram of a Schwarzschild black hole, plotting radial distance r against time t_*. Some radial null geodesics (photon trajectories) and lightcones are shown. The event horizon is the dashed line at $r = 2M$. The curvature singularity is the red line at $r = 0$. [20]

2.2 Black Hole Thermodynamics

The first two laws of black hole mechanics [21], established by Carter, Hawking, and Bardeen are

$$\begin{aligned} &\text{(i)} \qquad dE = \frac{\kappa}{8\pi} dA + dW, \\ &\text{(ii)} \qquad \frac{dA}{dt} \geq 0, \end{aligned} \tag{2.1}$$

where E is the energy of the black hole, κ the surface gravity, A the horizon area, W the work done on the black hole (due to its charge or spin) and t is time. In words, the first law states that the change of energy of a black hole is caused by either a change of its size or work done on it. The second law states that the area of the horizon cannot decrease.

The first two laws of thermodynamics are

$$\begin{aligned} &\text{(i)} \qquad dE = TdS + dW, \\ &\text{(ii)} \qquad \frac{dS}{dt} \geq 0, \end{aligned} \tag{2.2}$$

where T is temperature, S is entropy and all other symbols have the same meaning as above [22]. Thus both sets of laws have similar forms, with A in some sense playing the same role as S.

By arguing that a black hole must both satisfy the first law of thermodynamics whilst also ensuring that the entropy of the entire universe cannot decrease, Bekenstein reasoned that a black hole must have an entropy proportional to its area [3, 23]. Hawking then found [4, 24] the proportionality constant to be $1/4$, where A is measured in Planck units, yielding the Bekenstein-Hawking entropy S_{BH} of a black hole

$$S_{BH} = \frac{1}{4} \frac{A}{l_P^2}, \tag{2.3}$$

where l_P is the Planck length, equal to

$$l_P = \sqrt{\frac{G\hbar}{c^3}} \approx 1.616229(38) \times 10^{-35} \text{ m} \tag{2.4}$$

in SI units [25]. So black hole entropy is related to quantum mechanics (because of $\hbar$) and gravity (because of G), within general relativity (because of c), making it an invaluable physical property to investigate in order to understand quantum gravity [26, 27].

2.3 What is Black Hole Entropy?

The Bekenstein-Hawking entropy's scaling with the horizon area suggests it is physically related to the horizon. Schematically, the horizon of a black hole can be thought to be made of tiles of area $4l_P^2$, where each tile represents one unit of entropy, as pictured in figure 2.2 [28]. Thus, the total entropy equals the number of these horizon tiles, each of which can be interpreted as a degrees of freedom (dof) of the horizon [7].

As discussed in section 2.1, the event horizon is just a boundary in spacetime, there is nothing physically there apart from spacetime itself. This suggests that horizon dofs must be dofs of spacetime. In order to motivate the notion of spacetime dofs, consider the entropy of a black hole due to quantum entanglement [30]. The entanglement entropy of a black hole encapsulates the hidden information inside the horizon that is entangled with information outside. Performing the quantum field theory (QFT) calculation on a black hole background,

within the continuum of GR, yields an infinite result for the entropy, contradicting S_{BH} in equation (2.3). However, performing the same calculation with a short distance cutoff l applied to the quantum modes yields a finite result for the entanglement entropy

$$S_E = k\frac{A}{l^2}, \tag{2.5}$$

where k is an undetermined constant of order 1 [31]. Thus, if spacetime where fundamentally discrete, with fundamental discreteness length l_f, the entanglement entropy can be written as

$$S_E = k\frac{A}{l_f^2} \equiv N_f, \tag{2.6}$$

where N_f can be thought of as the number of fundamental spacetime dofs belonging to the horizon [7]. By equating S_{BH} from equation (2.3) with S_E one finds

$$\frac{1}{4}\frac{A}{l_P^2} = k\frac{A}{l_f^2} \tag{2.7}$$

$$\left(\frac{l_f}{l_P}\right)^2 = 4k. \tag{2.8}$$

Therefore calculating k within a theory of quantum gravity will determine the value of l_f, which in turn could provide a natural explanation for why constants of nature such as G and $\hbar$ have the values that they do.

A question that remains is what do spacetime dofs physically represent? The remainder of this report will investigate an answer proposed within causal set theory.

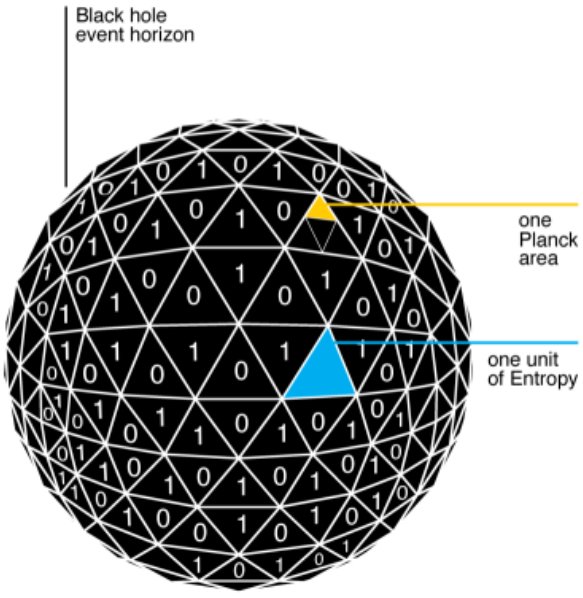

Figure 2.2: Tiled event horizon. Each (blue) entropy tile corresponds to one unit of entropy. Each unit of entropy can be interpreted as one bit of information (i.e. 1 dof), hence the 0 or 1 on each entropy tile. [29]

Chapter 3

Causal Set Theory

During the 1970-80s, the notion of discrete spacetime, together with the importance of causal order, was hypothesized independently by various physicists [5, 32, 33] and amalgamated with the creation of a theory of quantum gravity known as causal set theory (CST). A key motivation for discrete spacetime is its prevention of many divergent physical quantities, including QFT amplitudes and the entanglement entropy of a black hole (as discussed in section 2.3) [34].

3.1 Causal Structure

Causal order is a key part of GR. Every event in spacetime has a causal future and past; every event can only influence, or be influenced by, specific other events. For two spacetime points, x and y, the order relation $x \leq y$ implies that y is in the causal future of x [35]. Every point x has a set of points in its causal future $J^+(x)$ and its causal past $J^-(x)$, as shown in figure 3.1.

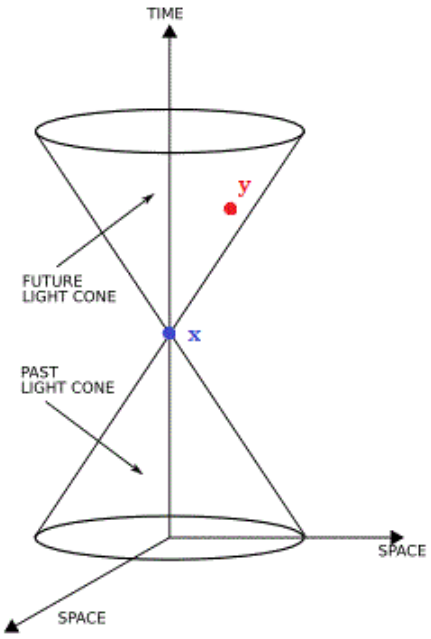

Figure 3.1: The causal past and future of x are all the points within the past and future lightcones of x respectively. Note, $y \in J^+(x)$.

Work in global causal analysis [36–41] has suggested that knowing the causal structure of a spacetime, that is knowing the order relations between every point, is enough to determine all of the spacetime's geometrical properties *if* one also had independent knowledge of the volume element. If spacetime were discrete, the volume of a region of spacetime is given by the

number of discrete elements corresponding to that region [42]. Volume information is encoded in the discretum and thus, if spacetime were discrete, causal order alone entirely determines the geometry of spacetime. In the words of Rafael Sorkin "Number + Order = Geometry" [43]. This unification provided by causal structure is a major motivation to treat it as fundamental within a discrete theory.

3.2 Mathematics of CST

A causal set (causet) is a locally finite partially ordered set [44]. Mathematically, it is a set $\mathcal{C}$ together with a binary relation $\preceq$ satisfying the following axioms:

(i) $x \preceq x, \forall x$ (reflexivity);

(ii) $x \preceq y \preceq z \Rightarrow x \preceq z, \forall\ x, y, z \in \mathcal{C}$ (transitivity);

(iii) $x \preceq y$ and $y \preceq x \Rightarrow x = y, \forall\ x, y \in \mathcal{C}$ (acyclicity);

(iv) $|\{y \in \mathcal{C} | x \preceq y \preceq z\}| < \infty, \forall\ x, z \in \mathcal{C}$ (local finiteness).

Furthermore, $x \prec y$ signifies that $x \preceq y$ and $x \neq y$. In words, $x \prec y$ means "x causally precedes y". Axioms (ii) and (iii) imply that the set is ordered. Axiom (iv) ensures discreteness [35, 45].

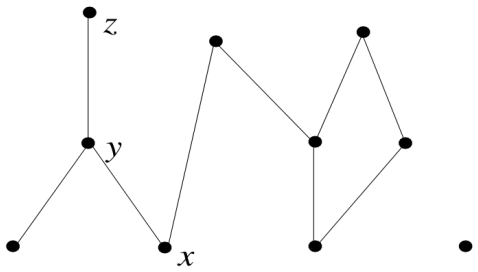

Figure 3.2: A Hasse diagram. Nodes represent causet elements and edges (lines) represent links. Links are drawn between nearest neighbours, thus, although $x \prec z$, there is no edge directly between x and z. Time increases upwards. [46]

Figure 3.2 depicts a visualisation of a causet, known as a Hasse diagram [46]. This is akin to an upside down family tree, following the convention that the time axis points upwards in relativity. Each node represents an element and the edges represent causal relations between nearest neighbours. A nearest neighbour relation is known as a *link* and is denoted by a $\prec *$ symbol. Thus, figure 3.2 depicts a causet $\mathcal{C} = \{x, y, z, ...\}$, where $x \prec * y \prec * z$. Note $x \prec z$ is not a link, because x and z are not nearest neighbours as y is in between. The diagram contains no notion of length – a causet is simply a set of elements with an order relation [45].

An element in a causet is *minimal* if there are no elements in the causet that are in its past. In figure 3.2, x is a minimal element of $\mathcal{C}$. This is written as $x \underline{\in} \mathcal{C}$. Similarly a *maximal* element contains no elements in its future. In the figure, z is maximal in $\mathcal{C}$, denoted $z \overline{\in} \mathcal{C}$ [16].

3.3 Continuum Correspondence

According to CST, the continuum does not exist. It is merely an approximation to a causet at scales much larger than the discreteness scale. If a continuum spacetime is a good approximation to a causet, then the causet will *faithfully embed* into the spacetime. Research is still

being performed to find properties of the continuum from an arbitrary causet [47–59], however a method of working backwards is known. Given a continuum spacetime, one can find a causet which faithfully embeds into it by performing a *sprinkling* [46], in which points from the continuum are randomly selected according to a Poisson process [60].

The Poisson process works as follows. Given an arbitrary region of spacetime R of volume V, the number of elements N in a faithfully embedded causet is a Poisson-distributed random variable [61]. Thus

$$\text{Prob}(N = k) = \text{Po}(k; \rho V) := \frac{(\rho V)^k e^{-\rho V}}{k!}, \tag{3.1}$$

where $\rho := l_f^{-n}$ is the density of sprinkling and n is the dimensionality of R. The N elements each correspond to a point in R and are distributed uniformly (sprinkled) throughout R. The causal relations can then be determined using the causal structure of R. A Poisson process both respects Lorentz invariance and ensures that, on average, $N \propto V$ so that "Number + Order = Geometry" [46]. Figure 3.3 illustrates sprinkling in the case of flat $2d$ spacetime.

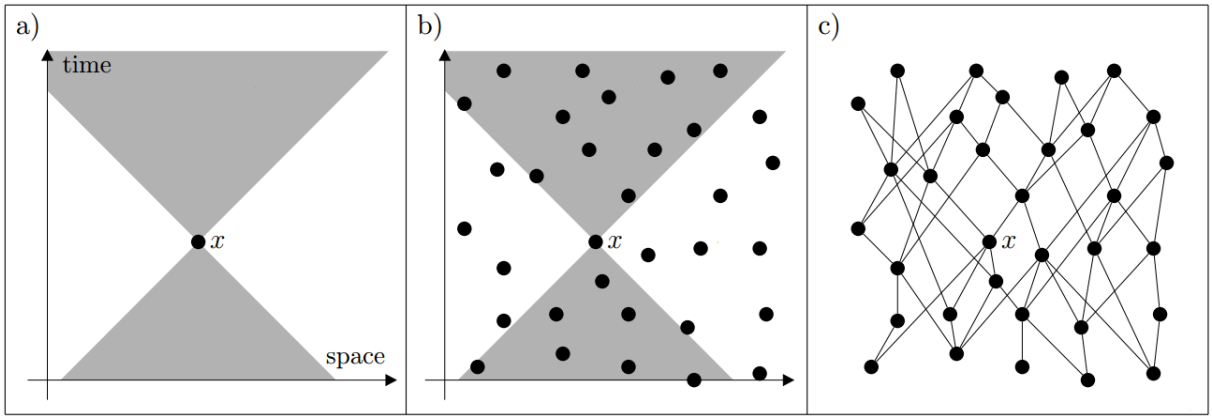

Figure 3.3: An illustration of sprinkling. (a) depicts a flat $2d$ continuum spacetime and signifies an arbitrary point x with its causal past and future (grey). (b) shows a set of sprinkled points (of which x is one), whose number and position were determined randomly according to a Poisson process. (c) depicts the causet (as a Hasse diagram) obtained from the sprinkling; each causet element corresponds to a sprinkled point and the links are determined by considering the causal order of each sprinkled point. This causet faithfully embeds into flat spacetime. [62]

3.4 Molecules and Counting Links

Figure 3.4 shows examples of two types of causet molecule: a link and a triplet. A key concept throughout this work will be counting molecules obtained through sprinkling. Because sprinkling is a random process, the quantity of interest is the average number of molecules over all possible sprinklings $<N_M>$. This section will specifically address the average number of links $<N_{\mathcal{L}}>$.

In order to calculate $<N_{\mathcal{L}}>$, the probability that a sprinkled point exists at a certain place in the continuum must be calculated. Using equation (3.1), the probability that one sprinkled point exists in a flat[1] n-dimensional volume element $d^n x$ is

$$\text{Po}(1; \rho d^n x) = \rho d^n x. \tag{3.2}$$

[1]This can be generalise to an arbitrary geometry, but this work only considers flat spacetime.

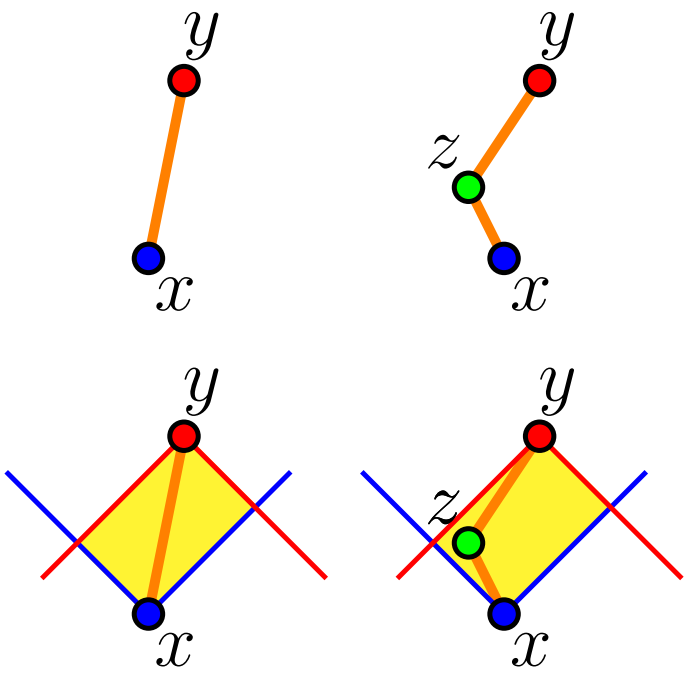

Figure 3.4: A link (top left) and triplet (top right), where x, y and z are sprinkled causet elements. Links are drawn in orange. The bottom pictures show the future lightcone of x and the past lightcone of y in blue and red respectively. The causal interval of x and y (yellow) contains no sprinkled points on the left and one sprinkled point (z) on the right.

Consider two sprinkled points x and y such that $x \in \mathcal{X}$ and $y \in \mathcal{Y}$, where $\mathcal{X}$ and $\mathcal{Y}$ are arbitrary regions within the sprinkled spacetime. If $x \prec\!* \, y$, there must be no other sprinkled points within $J^+(x) \cap J^-(y)$, known as the causal interval of x and y, as shown in figure 3.4. If there were a point in this region, x and y would no longer be linked as they would no longer be nearest neighbours. Therefore, the probability that x and y are linked equals the probability that $J^+(x) \cap J^-(y)$ is empty. Using equation (3.1), this is given by

$$\mathrm{Po}[0; \rho V_{\mathcal{L}}(x,y)] = e^{-\rho V_{\mathcal{L}}(x,y)}, \tag{3.3}$$

where $V_{\mathcal{L}}(x,y)$ is the volume of $J^+(x) \cap J^-(y)$.

Therefore the probability of there being a point x in $d^n x$ and another point y in $d^n y$ and that x-y is a link, is given by

$$P(x \prec\!* \, y) := \mathrm{Po}(1; \rho d^n x)\ \mathrm{Po}(1; \rho d^n y)\ \mathrm{Po}[0; \rho V_{\mathcal{L}}(x,y)] = \rho d^n x\ \rho d^n y\ e^{-\rho V_{\mathcal{L}}(x,y)}. \tag{3.4}$$

The presence or non-presence of a link is a binary outcome, thus $<N_{\mathcal{L}}>$ is given by a sum of $P(x \prec\!* \, y)$ over all link possibilities. Specifically, in the infinitesimal volume element limit, the expected number of links $x \prec\!* \, y$ between $\mathcal{X}$ and $\mathcal{Y}$ is given by integrating $P(x \prec\!* \, y)$ throughout $\mathcal{X}$ and $\mathcal{Y}$, whilst ensuring that y is in the future of x. Therefore,

$$<N_{\mathcal{L},n}> \; = \sum_{x\text{-}y \text{ pairs}} P(x \prec\!* \, y) \to \int_{\mathcal{X}} \rho d^n x \int_{\mathcal{Y} \cap J^+(x)} \rho d^n y\ e^{-\rho V_{\mathcal{L}}(x,y)}, \tag{3.5}$$

where the subscript n explicitly shows dimensional dependence. The exponent of the exponential is a key property of this equation. For a given ρ, the smaller $V_{\mathcal{L}}(x,y)$, the more likely x and y are linked. If $V_{\mathcal{L}}(x,y) \approx 0$ for a large set of x-y pairs, then $<N_{\mathcal{L}}>$ will be large [63]. Figure 3.5 shows a sketch of the link counting setup in $2d$.

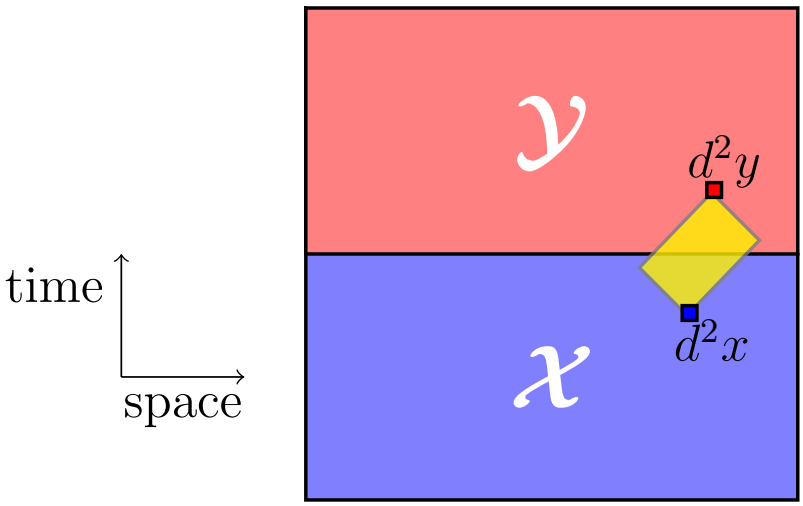

Figure 3.5: Illustration of link counting in a $2d$ sprinkling. The average number of links between regions $\mathcal{X}$ and $\mathcal{Y}$ is given by considering the probability of the presence of linked pairs between each infinitesimal volume element pair (d^2x and d^2y). The yellow rectangle is the causal interval of the volume element pair.

Chapter 4

Black Hole Entropy in Causal Set Theory

Sprinkling can be performed on any spacetime, including one containing a black hole. In such a sprinkling, causet molecules will intersect the event horizon. Sorkin proposed that, to a first approximation, the horizon dofs are causet molecules intersecting the horizon [14, 15]. This will now be discussed in the context of the event horizon of a collapsing shell of matter.

4.1 A Collapsing Shell of Matter

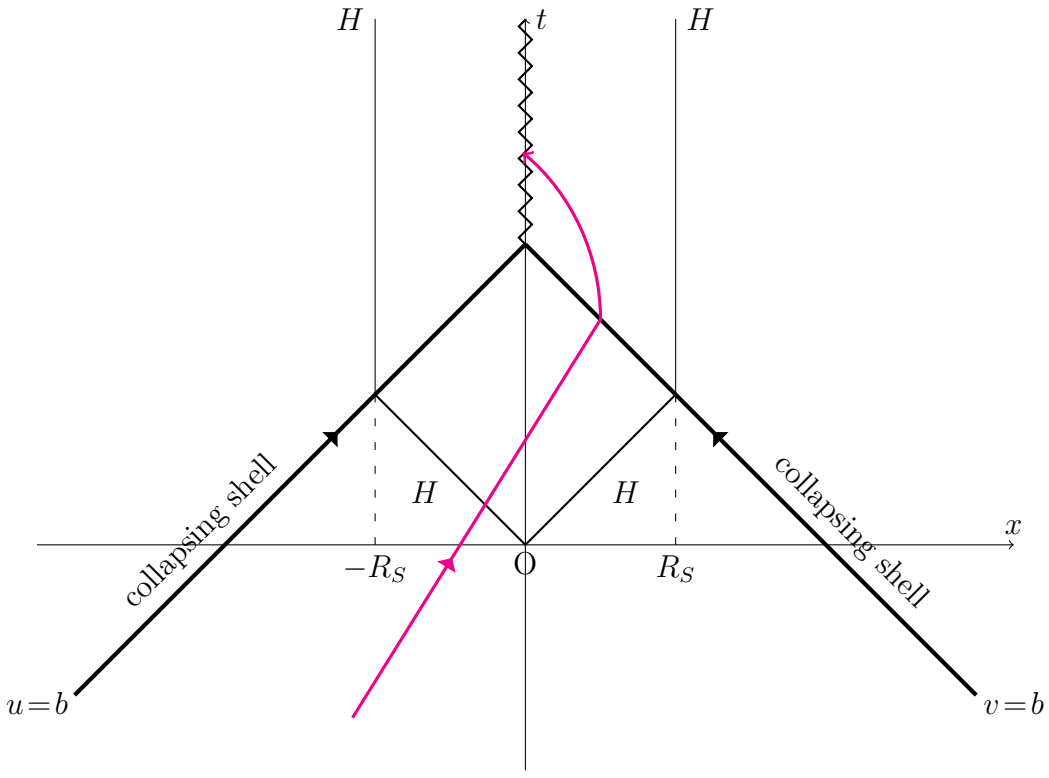

Figure 4.1: A $1+1D$ spacetime diagram of a collapsing shell in Cartesian coordinates (t, x) with origin O. The thick black line at lightcone coordinate b is the collapsing shell. The horizon H comprises of the thin solid lines. The zigzagged line represents the $r = 0$ curvature singularity. A possible particle trajectory is drawn in magenta, illustrating that, even during the collapse, an event horizon exists within which no matter can ever escape.

One way a black hole can form is via the collapse of a massive object, such as a star, which can be modelled as a spherical shell of matter [15]. Consider a spherical shell of matter in a

vacuum, collapsing over time. Working in Cartesian coordinates (t, x, y, z), this corresponds to a spherical shell in the space described by the x, y and z coordinates, decreasing in radius as t increases. Therefore, the (t, x) plane contains two antipodal points on the shell (at $y = z = 0$) moving towards each other over time, as pictured in figure 4.1.

Using lightcone coordinates (v, u), defined as

$$v := \frac{t + x}{\sqrt{2}}, \qquad u := \frac{t - x}{\sqrt{2}}, \tag{4.1}$$

the trajectory of the collapsing shell is chosen to be along $v = b$ for $x > 0$ and $u = b$ for $x < 0$, where b is a constant. These are straight lines of gradient ± 1 in the (t, x) plane.

It can be seen in figure 4.1 that there are two parts to the horizon. Firstly, a horizon exists during the collapse; whilst the shell is larger than R_S, a 'V-shaped' horizon can be seen to exist inside the shell. Moreover, after the shell has collapsed, the horizon has a constant value of $r = |x| = R_S$; at this point a static black hole has formed, thus this looks similar to figure 2.1. The spacetime inside the shell is flat, whereas outside is curved, therefore analytical calculations concerning the horizon inside the shell are significantly simpler [14, 15]. Hence it is this horizon that will be studied throughout this work.

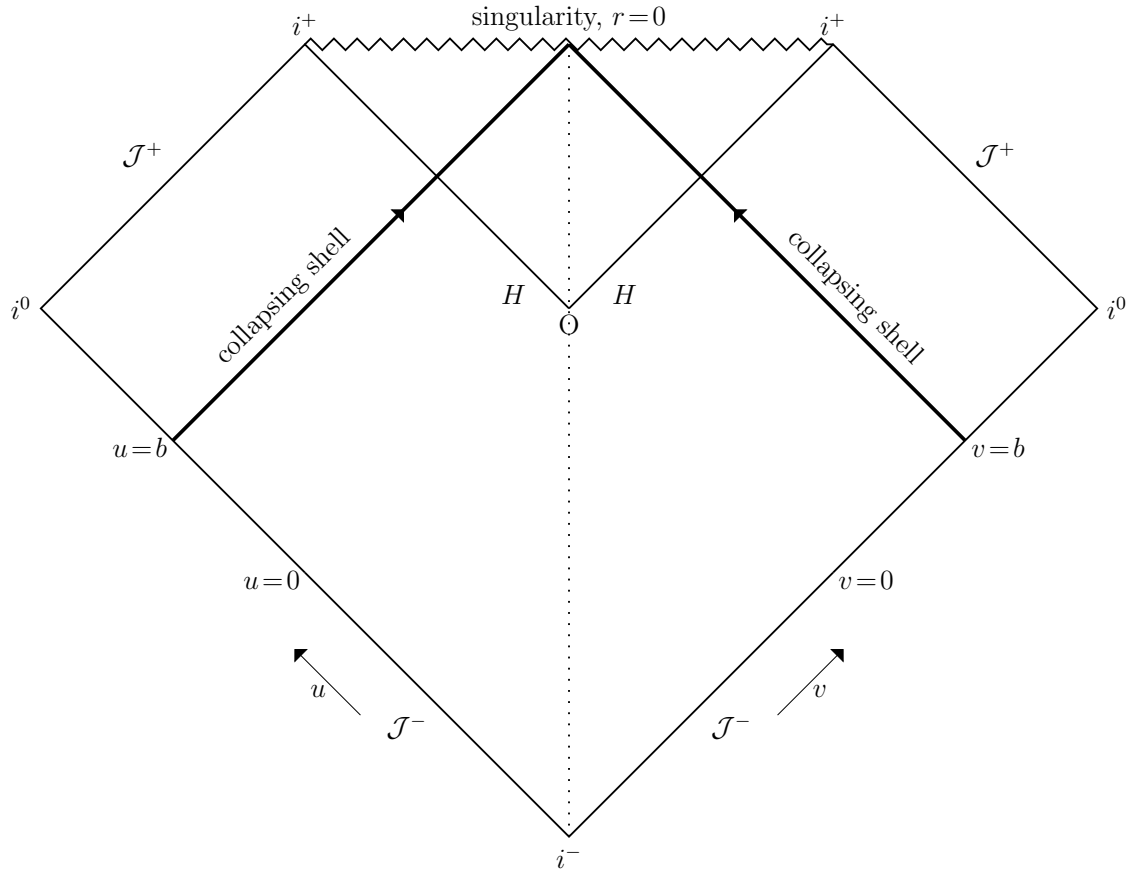

Figure 4.2: Penrose diagram of a collapsing shell at lightcone coordinate b with horizon H. Lightcone coordinate axes have been included to show the analogy with figure 4.1 inside the shell. All other symbols accord with Penrose diagram conventions [18]. The vertices $i^{\pm}$ represent lightcone coordinates $(\pm\infty, \pm\infty)$. The right edge (between i^- and i^0) represents $u = -\infty$, and the opposite, left, edge represents $v = -\infty$; both of these are denoted by $\mathcal{J}^-$.

This collapsing shell can be depicted as a Penrose diagram [18], which reduces infinite spacetime to a finite size picture. In a Penrose diagram, lightcones are always straight lines at 45° to the vertical, regardless of the spacetime's curvature. Hence figure 4.2 differs from figure

4.1 in the fact the horizon is now always at 45° to the vertical and the singularity is now a horizontal line. Because the flat interior of the shell looks the same in both figures, one can analogously think in terms of lightcone coordinates, i.e. (v, u) coordinates with origin O, inside the shell.

4.2 Entropy Equals Number of Horizon Molecules

Entropy is a quantity that is calculated at a given time, therefore a null hypersurface, denoted Σ, is introduced to the Penrose diagram at lightcone coordinate a, as in figure 4.3. Note, in the (t, x) plane, a null hypersurface is two straight lines of gradient ± 1. The entropy of the horizon H will be calculated at the time at which Σ intersects H (denoted $H \cap \Sigma$). It is proposed that

> the entropy of a black hole at time signified by Σ is, to first order, equal to the number of molecules that intersect both H and Σ whilst remaining local to $H \cap \Sigma$.

The regions of locality are illustrated in figure 4.3 by green circles; molecules must lie within a green circle to be local. This proposal is akin to thermodynamics, where the entropy of a box of gas is proportional to the number of molecules in the box [64].

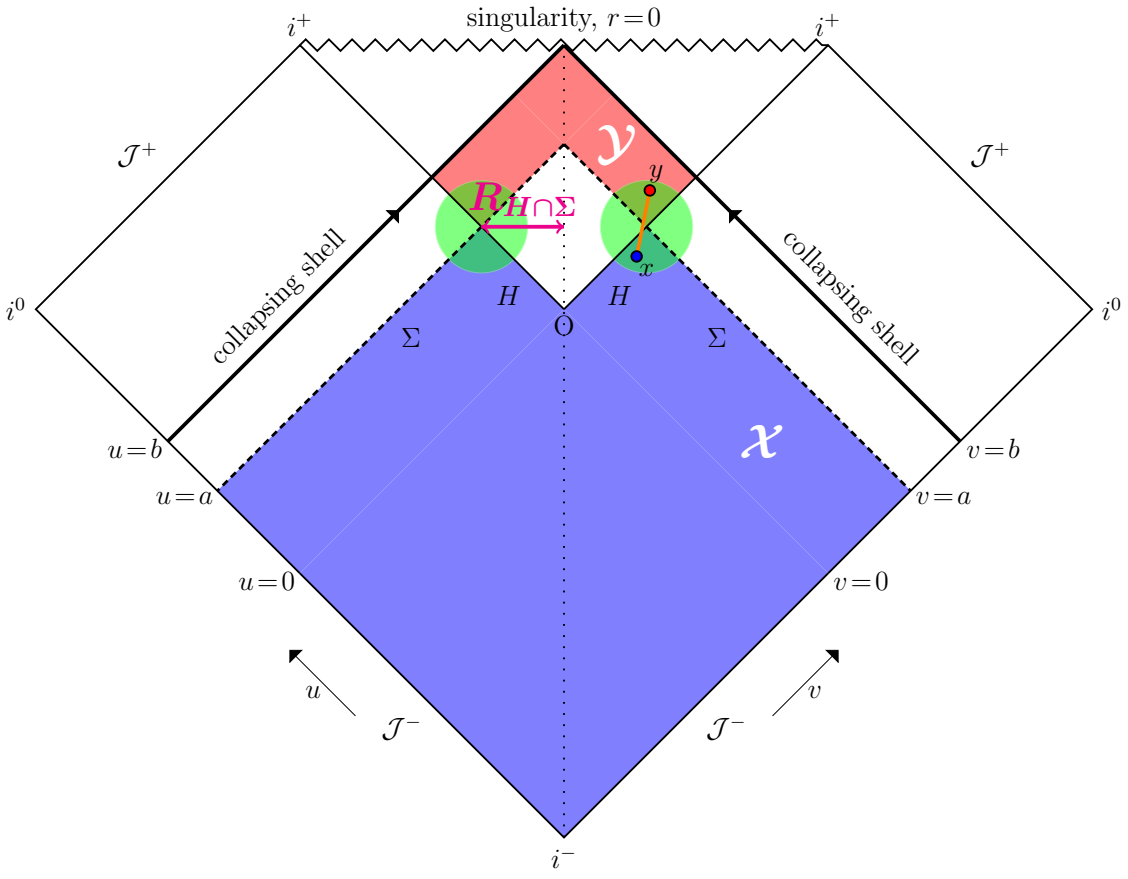

Figure 4.3: Penrose diagram of collapsing shell (figure 4.2). Two dashed lines representing Σ are added at lightcone coordinate a. $\mathcal{X}$ is the blue region and $\mathcal{Y}$ the red region. Green circles illustrate where molecules must lie in order to be local. A local link $x \prec * y$ is shown. In this $2d$ picture, $H \cap \Sigma$ corresponds to the two points at which H intersects Σ (a 0-sphere). $R_{H\cap\Sigma}$, the radius of $H \cap \Sigma$, is the length of the magenta line.

To calculate the expected number of links $<N_{\mathcal{L},n}>$ using equation (3.5), the regions $\mathcal{X}$ and $\mathcal{Y}$ must be specified. Note, although equation (3.5) applies to links, a similar integral applies

to all molecules we will consider. To ensure that molecules cross both H and Σ, we choose

$$\begin{aligned} \mathcal{X} &:= J^-(H) \cap J^-(\Sigma), \\ \mathcal{Y} &:= J^+(H) \cap J^+(\Sigma) \cap J^-(shell). \end{aligned} \tag{4.2}$$

This is depicted in figure 4.3. Because entropy is a physical property of a black hole, it must be defined covariantly, which is ensured by defining $\mathcal{X}$ and $\mathcal{Y}$ solely in terms of causal structure.

4.2.1 The Macroscopic Regime

This work considers the horizon within the shell only and will therefore take $a \ll b$, such that the shell is far away from the time at which entropy is calculated. Furthermore, a macroscopic black hole, far larger than the discreteness scale, will be considered by taking $l_f \ll a$. Together these define the *macroscopic regime* $l_f \ll a \ll b$, or equivalently, $1 \ll \rho a^n \ll \rho b^n$, where n is the dimensionality of spacetime. To investigate the macroscopic regime one can either fix ρ and make a and b sufficiently large, or alternatively fix a and b whilst increasing ρ [15].

4.2.2 Criteria for Agreement with S_E

Mathematically, the proposal says that

$$<N_{M,4}> \simeq S_E \tag{4.3}$$

$$= k\frac{A_2}{l_f^2}, \tag{4.4}$$

where equation (2.6) was used for S_E and A_2 is the area of $H \cap \Sigma$ (the subscript 2 is used to signify this is the area of a 2-sphere [65], i.e. a spherical shell). Note that this proposal does not specify which molecules M correspond to the entropy. Therefore this work investigates which, if any, molecules do satisfy it and are thus *horizon molecules*.

Calculations in $4d$ are difficult, therefore, as a first attempt to test the proposal, this work will perform calculations in lower dimensions. An n-dimensional analogue of equation (4.4) is

$$<N_{M,n}> \simeq k_n \frac{A_{n-2}}{l_f^{n-2}}, \tag{4.5}$$

where $<N_{M,n}>$ is the number of molecules in a sprinkling on an n-dimensional cut of the $4d$ spacetime, k_n is a dimension dependant constant of order unity and A_{n-2} is the area of the $(n-2)$-sphere [65] corresponding to $H \cap \Sigma$.

A $3d$ slice of the shell at constant spherical polar angle θ contains a circular ring (a 1-sphere) of the shell collapsing over time. This slice corresponds to fully rotating the Penrose diagram in figure 4.3 about the dotted vertical. Therefore $A_1 = 2\pi R_{H\cap\Sigma}$ is the circumference of the circular ring, where $R_{H\cap\Sigma}$ is the radius of $H \cap \Sigma$. Using this, together with $l_f = \rho^{-1/n}$, gives

$$<N_{M,3}> \simeq k_3 \; 2\pi R_{H\cap\Sigma} \; \rho^{1/3}. \tag{4.6}$$

It can be seen in figure 4.3 that because $H \cap \Sigma$ is a distance a from the origin, $R_{H\cap\Sigma} = a/\sqrt{2}$. Therefore,

$$<N_{M,3}> \simeq k_3 \; \sqrt{2}\pi a \; \rho^{1/3}. \tag{4.7}$$

Alternatively, slicing on the (t, x) plane gives a $2d$ slice which must obey

$$<N_{M,2}> \simeq k_2 \frac{A_0}{l_f^0} = 2k_2 \sim 1. \tag{4.8}$$

Note A_0 is the area of a 0-sphere [65], which is two points and therefore equals 2. This slice is what the Penrose diagram depicts.

Note the use of '$\simeq$', implying these must be the leading order contributions in the macroscopic regime.

4.2.3 Criterion for Locality

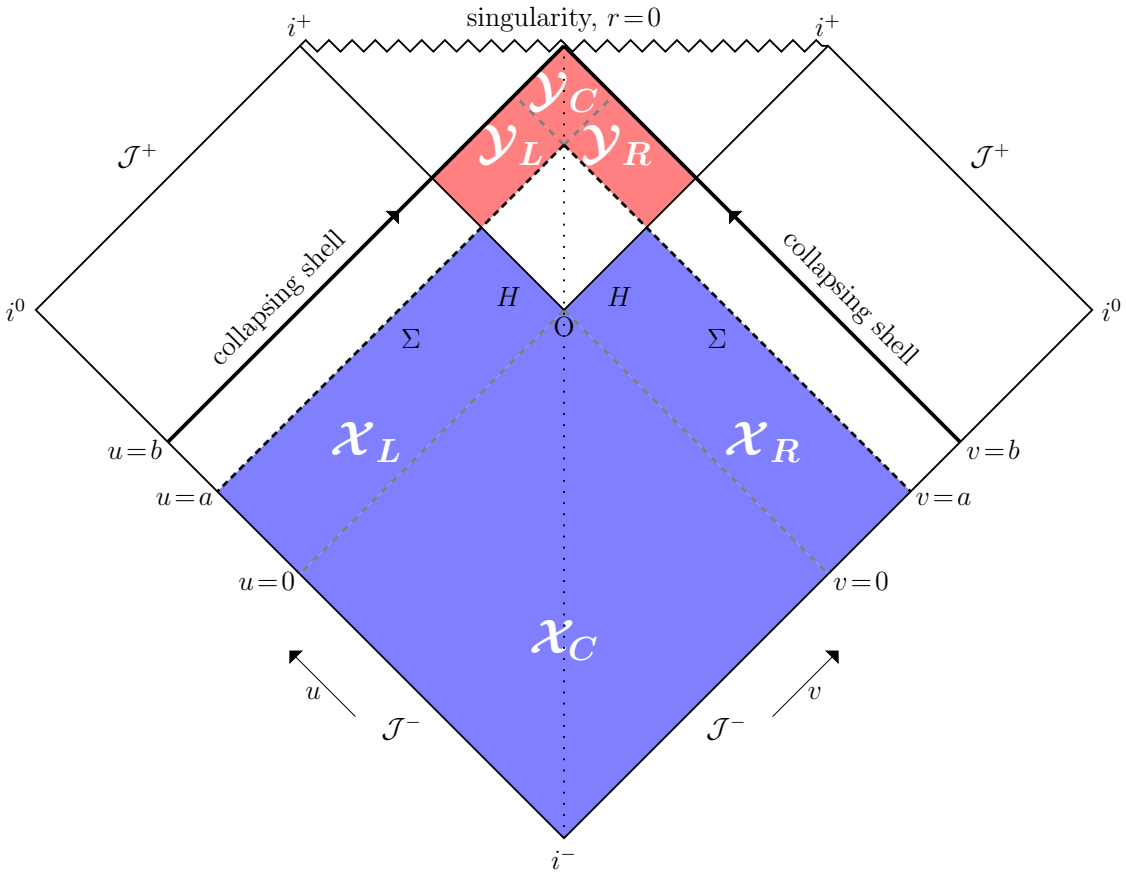

Figure 4.4: Penrose diagram of collapsing shell (figure 4.3). $\mathcal{X}_L$, $\mathcal{X}_C$, $\mathcal{X}_R$, $\mathcal{Y}_L$, $\mathcal{Y}_C$ and $\mathcal{Y}_R$ are shown between the dashed grey lines. Also, note the mirror symmetry in the dotted vertical line.

As shown in figure 4.4, $\mathcal{X}$ can be split into 3 subregions, $\mathcal{X}_R$, $\mathcal{X}_L$ and $\mathcal{X}_C$, where the subscripts mean right, left and central, respectively. $\mathcal{Y}$ can be split similarly. Thus, $<N_{\mathcal{L},n}>$ can be written

$$<N_{\mathcal{L},n}> = \left(\int_{\mathcal{X}_R} + \int_{\mathcal{X}_L} + \int_{\mathcal{X}_C}\right) \rho\, d^n x \left(\int_{\mathcal{Y}_R \cap J^+(x)} + \int_{\mathcal{Y}_L \cap J^+(x)} + \int_{\mathcal{Y}_C \cap J^+(x)}\right) \rho\, d^n y\, e^{-\rho V_{\mathcal{L}}(x,y)}. \tag{4.9}$$

This can be expanded into nine integrals, however, if links are local they will not reach the central regions, or extend from the left to the right half of spacetime. The green circles only connect $\mathcal{X}_R$ to $\mathcal{Y}_R$ and $\mathcal{X}_L$ to $\mathcal{Y}_L$, thus these two contributions alone include all local contributions. Hence, a necessary but not sufficient condition for locality is

$$<N_{\mathcal{L},n}> \simeq \int_{\mathcal{X}_R} \rho\, d^n x \int_{\mathcal{Y}_R \cap J^+(x)} \rho\, d^n y\, e^{-\rho V_{\mathcal{L}}(x,y)} + \int_{\mathcal{X}_L} \rho\, d^n x \int_{\mathcal{Y}_L \cap J^+(x)} \rho\, d^n y\, e^{-\rho V_{\mathcal{L}}(x,y)}, \tag{4.10}$$

with the seven other integrals contributing negligibly. Note this is not sufficient because the green circles are smaller than $\mathcal{X}_R$ and all other subregions.

Because the Penrose diagram (see figure 4.4) is symmetric across the dotted vertical, there is an $R \leftrightarrow L$ symmetry, thus the above two terms are equal. Moreover, if $x \in \mathcal{X}_R$ then $\mathcal{Y}_R \cap J^+(x) = \mathcal{Y}_R$, so the locality condition becomes

$$<N_{\mathcal{L},n}> \simeq 2 \int_{\mathcal{X}_R} \rho \, d^n x \int_{\mathcal{Y}_R} \rho \, d^n y \, e^{-\rho V_{\mathcal{L}}(x,y)} =: 2 <N^{RR}_{\mathcal{L},n}>, \tag{4.11}$$

where $<N^{RR}_{\mathcal{L},n}>$ is the contribution between $\mathcal{X}_R$ and $\mathcal{Y}_R$, the *right-right contribution.*

The symmetry discussed above is related to spacetime, not the molecule, therefore

$$<N_{M,n}> \simeq 2 \int_{\mathcal{X}_R} \rho \, d^n x \int_{\mathcal{Y}_R} \rho \, d^n y \, P_M(x,y) =: 2 <N^{RR}_{M,n}> \tag{4.12}$$

is the locality condition for any molecule M, provided the appropriate integrand $P_M(x,y)$ is inserted.

4.2.4 Symmetry

If molecules are local there is an $\mathcal{X} \leftrightarrow \mathcal{Y}$ symmetry, although this is an approximate symmetry as it only applies in the macroscopic regime. Figure 4.5 shows the axis of this mirror symmetry, which arises when $\mathcal{Y}$ is sufficiently large that it is effectively the same size as $\mathcal{X}$ as far as local molecules are concerned.

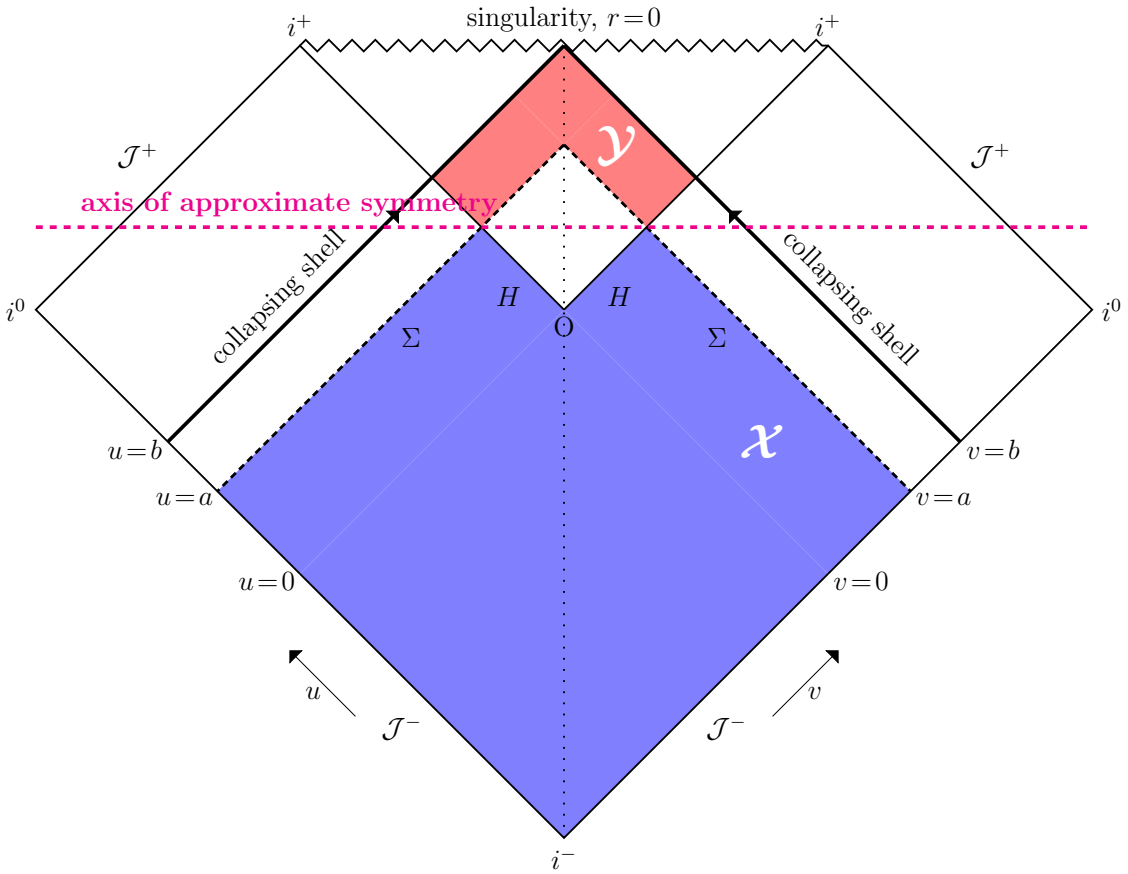

Figure 4.5: Penrose diagram of null collapsing shell (figure 4.3) showing the horizontal axis of approximate $\mathcal{X} \leftrightarrow \mathcal{Y}$ symmetry.

Chapter 5

Counting Links in $1+1D$

The simplest type of molecule is a link, this will be the first molecule to be investigated. A link crossing the horizon can be thought of as a flow of information from the exterior to the interior of the horizon, fitting in well with the notion of entanglement entropy. We will now refer to the previously defined link as a *plain link* for reasons that will become clear.

5.1 The Right-Right Contribution

5.1.1 Plain Links

To start, consider $<N^{RR}_{\mathcal{L},2}>$ as defined in equation (4.11). Figure 5.1 shows both integration regions, $\mathcal{X}_R$ and $\mathcal{Y}_R$, together with $V_{\mathcal{L}}(x,y)$. By considering the lightcone coordinate annotations on the Penrose diagram, it can be seen that $\mathcal{X}_R$ extends from $u=-\infty$ to $u=0$ and $v=0$ to $v=a$, while $\mathcal{Y}_R$ extends from $u=0$ to $u=a$ and $v=a$ to $v=b$. These give the limits of integration. Also, by considering the area of the yellow rectangle, it can be seen that

$$V_{\mathcal{L}}(x,y) = (u_y - u_x)(v_y - v_x), \tag{5.1}$$

where u_x is the u coordinate of the point x (and similar). Thus integrating one by one gives

$$\begin{aligned}
<N^{RR}_{\mathcal{L},2}> &= \int_{\mathcal{X}_R} \rho\ d^2x \int_{\mathcal{Y}_R} \rho\ d^2y\ e^{-\rho V_{\mathcal{L}}(x,y)} \\
&= \rho^2 \int_a^b dv_y \int_0^a dv_x \int_{-\infty}^0 du_x \int_0^a du_y\ e^{-\rho(u_y-u_x)(v_y-v_x)} \\
&= \rho \int_a^b dv_y \int_0^a dv_x \int_{-\infty}^0 du_x\ \frac{e^{\rho u_x(v_y-v_x)}(1-e^{-\rho a(v_y-v_x)})}{v_y-v_x} \\
&= \int_a^b dv_y \int_0^a dv_x\ \frac{1-e^{-a\rho(v_y-v_x)}}{(v_y-v_x)^2} \\
&= \int_a^b dv_y\ \frac{1}{v_y(v_y-a)} \Big\{ a + e^{-\rho a v_y}(-a+v_y-v_y e^{\rho a^2}) \\
&\qquad\qquad \rho a v_y \Big[v_y \operatorname{Ei}(-\rho a v_y) - a \operatorname{Ei}(-\rho a v_y) \\
&\qquad\qquad - v_y \operatorname{Ei}\big(-\rho a(v_y-a)\big) + a \operatorname{Ei}\big(-\rho a(v_y-a)\big) \Big] \Big\} \\
&= \int_a^b dv_y\ \left\{ \frac{a}{v_y(v_y-a)} + \frac{e^{-\rho a v_y}}{v_y} - \frac{e^{-\rho a(v_y-a)}}{v_y-a} + \rho a \Big[\operatorname{Ei}(-\rho a v_y) - \operatorname{Ei}\big(-\rho a(v_y-a)\big) \Big] \right\}
\end{aligned}$$

$$= 1 + \gamma + \ln[\rho a^2] - \ln[\rho ab] + \ln[\rho a(b-a)] - e^{-\rho a^2} + e^{-\rho ab} - e^{-\rho a(b-a)}$$
$$- (1 + \rho a^2)\,\mathrm{Ei}[-\rho a^2] + (1 + \rho ab)\,\mathrm{Ei}[-\rho ab] - (1 + \rho a(b-a))\,\mathrm{Ei}[-\rho a(b-a)],$$

where $\mathrm{Ei}(x)$ is the exponential integral [66] and γ is the Euler-Mascheroni constant [67].

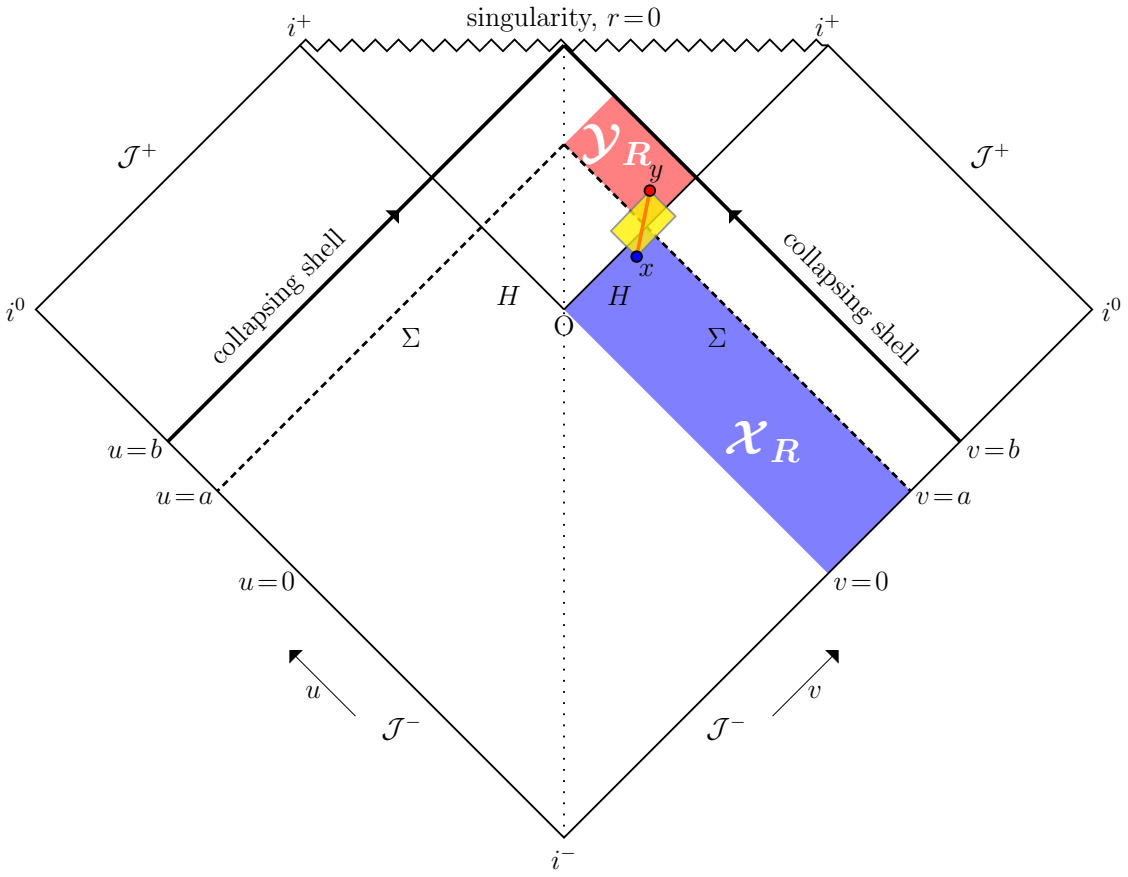

Figure 5.1: Penrose diagram (figure 4.4) illustration for $<N^{RR}_{\mathcal{L},2}>$ calculation, including causal interval (yellow).

The asymptotic expansion [68] of $\mathrm{Ei}(x)$,

$$\mathrm{Ei}(x) \sim \frac{e^x}{x} \sum_{k=0}^{\infty} \frac{k!}{x^k}, \tag{5.2}$$

establishes that terms of the form $(1 + x)\,\mathrm{Ei}(-x)$ are exponentially suppressed for large x. To investigate the leading order behaviour in the macroscopic regime, exponentially suppressed terms can be dropped, giving

$$<N^{RR}_{\mathcal{L},2}> \simeq 1 + \gamma + \ln[\rho a^2] - \ln[\rho ab] + \ln[\rho a(b-a)] \tag{5.3}$$
$$= 1 + \gamma + \ln\left[\rho a^2 \left(1 - \frac{a}{b}\right)\right] \tag{5.4}$$
$$= 1 + \gamma + \ln(\rho a^2) - \mathcal{O}\left(\frac{a}{b}\right) \tag{5.5}$$
$$\simeq \ln(\rho a^2) - \mathcal{O}\left(\frac{a}{b}\right). \tag{5.6}$$

Note that the Maclaurin expansion of $\ln(1 + x)$ was used in the penultimate step.

Thus the number of plain links is unbounded with a (and ρ). Increasing a corresponds to increasing the size of $\mathcal{X}_R$ and, if $b \gg a$, $\mathcal{Y}_R$. Therefore this result says that the number of links will increase indefinitely as $\mathcal{X}_R$ and $\mathcal{Y}_R$ are made larger, which is non-local behaviour. Moreover, this does not satisfy equation (4.8), suggesting plain links cannot be horizon molecules. This is heuristically understandable because $V_{\mathcal{L}}(x,y) \simeq 0$ whenever both x and y lie close to either H or Σ, regardless of how far away they are from $H \cap \Sigma$. This can be pictured by moving x and y in figure 5.1 and considering the change in size of the yellow rectangle. Therefore the integrand in equation (4.11), which is the probability that x and y are linked, will be large far away from $H \cap \Sigma$. Note that this conclusion was stated, without mathematical proof, by Dou in [14].

5.1.2 Constraining the Links

Given the failure of counting all links between $\mathcal{X}_R$ and $\mathcal{Y}_R$, a way of modifying the calculation to only consider links that lie locally to $H \cap \Sigma$ is required. We cannot simply integrate over the green circles of figure 4.3, as the green circles will change shape during a Lorentz transformation meaning a non-covariant definition of entropy. An alternative, covariant, constraint applied by Dou is to restrict $y \subseteq J^+(H)$ [14, 15], which means only count links whose y is minimal in the future of the horizon, forcing y to lie close to H. These links will be referred to as y-links.

This constraint requires that $J^+(H) \cap J^-(y)$ be empty, in addition to the causal interval of x and y required for plain links. Therefore a different integrand is required for this calculation, where $V_{\mathcal{L}}(x,y)$ is replaced by the volume that must be empty in order to ensure the above. The empty volume for y-links is shown in figure 5.2 and it can be seen that as y moves away from $H \cap \Sigma$the empty volume will become larger than for plain links, in turn suppressing non-local links. By calculating the areas of the yellow rectangles in figure 5.2, the new empty volume is

$$\begin{aligned} V_{\mathcal{L}y}(x,y) &= V_{\mathcal{L}}(x,y) + v_x u_y \\ &= u_x v_x + u_y v_y - u_x v_y. \end{aligned} \tag{5.7}$$

Thus the right-right contribution for y-links is given by

$$\begin{aligned} <N^{RR}_{\mathcal{L}y,2}> &= \int_{\mathcal{X}_R} \rho \; d^2x \int_{\mathcal{Y}_R} \rho \; d^2y \; e^{-\rho V_{\mathcal{L}y}(x,y)} \\ &= \rho^2 \int_a^b dv_y \int_0^a du_y \int_0^a dv_x \int_{-\infty}^0 du_x \; e^{-\rho(u_x v_x + u_y v_y - u_x v_y)} \\ &= \rho \int_a^b dv_y \int_0^a du_y \int_0^a dv_x \; \frac{e^{-\rho u_y v_y}}{v_y - v_x} \\ &= \rho \int_a^b dv_y \int_0^a du_y \; e^{-\rho u_y v_y} \ln\left(\frac{v_y}{v_y - a}\right) \\ &= \int_a^b dv_y \; \frac{1}{v_y}\left(1 - e^{-\rho a v_y}\right) \ln\left(\frac{v_y}{v_y - a}\right). \end{aligned} \tag{5.8}$$

Given $v_y \geq a$, then $e^{-\rho a v_y} \leq e^{-\rho a^2} \ll 1$ in the macroscopic regime, so the exponential in parentheses can be dropped for a highest order contribution calculation. This gives

$$<N^{RR}_{\mathcal{L}y,2}> \simeq -\int_a^b dv_y \; \frac{1}{v_y} \ln\left(1 - \frac{a}{v_y}\right) \tag{5.9}$$

$$= \mathrm{Li}_2(1) - \mathrm{Li}_2\left(\frac{a}{b}\right) \tag{5.10}$$

$$= \frac{\pi^2}{6} - \mathrm{Li}_2\left(\frac{a}{b}\right) \tag{5.11}$$

$$= \frac{\pi^2}{6} - \mathcal{O}\left(\frac{a}{b}\right) \tag{5.12}$$

to leading order in corrections, where $\mathrm{Li}_2(x)$ is the dilogarithm of x [69]. In the macroscopic regime this gives a contribution of order unity, hence if links are local and $<N_{\mathcal{L}y,2}> \simeq 2\ <N^{RR}_{\mathcal{L}y,2}>$, according to equation (4.11), then equation (4.8) is satisfied with $k_2 = \pi^2/6$. This is the conclusion of Dou and Marr in [14–16] without successful mathematical consideration of non-local contributions, which will now be analysed.

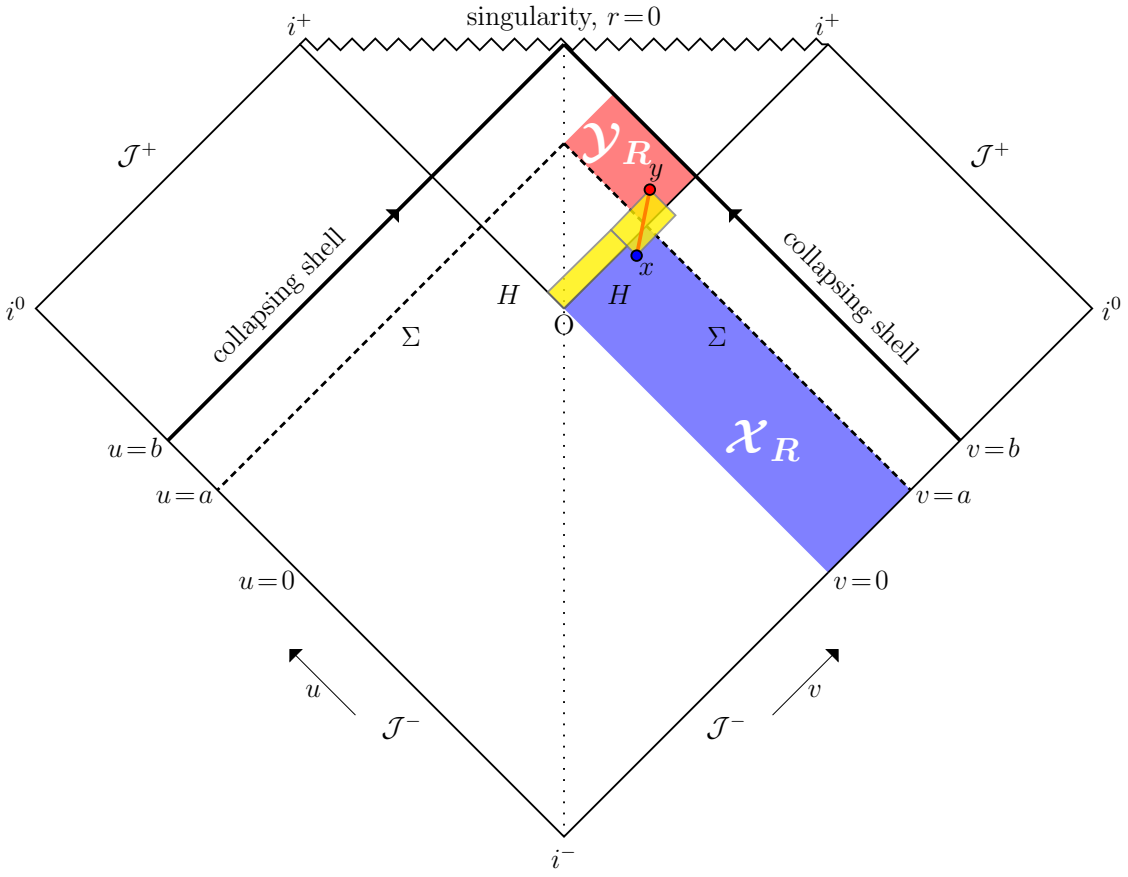

Figure 5.2: Penrose diagram (figure 4.4) illustration for $< N^{RR}_{\mathcal{L}y,2} >$ calculation, with empty volume shown in yellow.

5.2 The Non-Local Contributions

Although not detailed in this report, it can be shown that the non-local contribution for y-links as currently defined is not negligible. For example, y-links between $\mathcal{X}_C$ and $\mathcal{Y}_R$ can be shown to scale as $\ln b/a$ in the macroscopic regime.

The reason for this is that although y has been constrained, x has not. Locality can be ensured by constraining $x \overline{\in} \mathcal{X}$, as this requires there to be no points in $\mathcal{X}$ that are in the future of x, forcing x to lie towards the top of the $\mathcal{X}$ region. Note that this is not as strict as the constraint on $\mathcal{Y}$, but sufficient to ensure locality. This constraint has no effect on the right-right contribution and will thus be absorbed into our definition of the links previously mentioned in this chapter.

This was stated without proof by Dou and Marr, however we have verified it by calculating all terms in equation (4.9). To illustrate one such calculation, consider the expected number of

y-links between $\mathcal{X}_L$ and $\mathcal{Y}_R$, denoted $<N^{LR}_{\mathcal{L}y,2}>$. The Penrose diagram highlighting the relevant regions for this calculation is shown in figure 5.3. It can be seen that both constraints, $x \overline{\in} \mathcal{X}$ and $y \underline{\in} J^+(H)$, add to the causal interval in the empty volume, which is now

$$\begin{aligned} V^{LR}_{\mathcal{L}y}(x,y) &= V_{\mathcal{L}}(x,y) + u_x v_y - (a-u_y)v_x \\ &= (u_y - u_x)(v_y - v_x) + u_x v_y - (a-u_y)v_x \\ &= u_x v_x + u_y v_y - a v_x. \end{aligned} \tag{5.13}$$

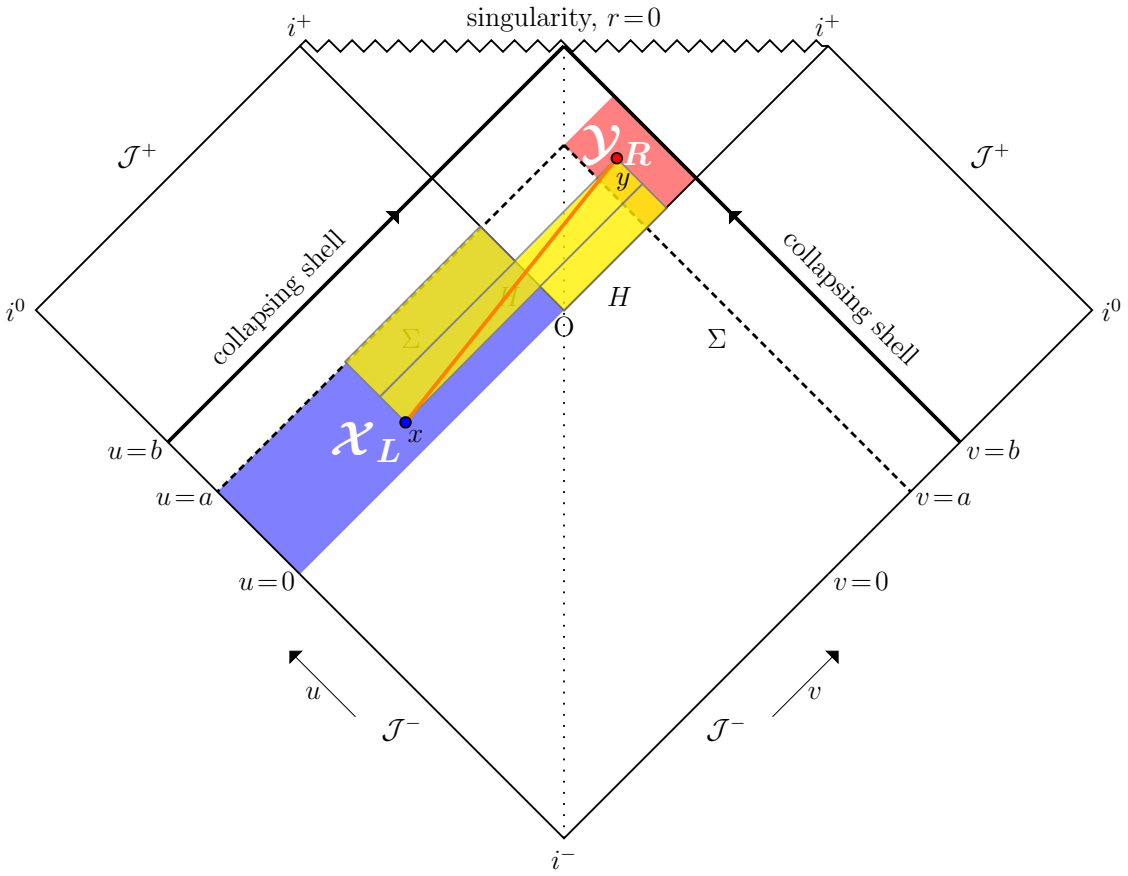

Figure 5.3: Penrose diagram (figure 4.4) illustration for $< N^{LR}_{\mathcal{L}y,2} >$ calculation, with empty volume shown in yellow.

Therefore,

$$\begin{aligned} <N^{LR}_{\mathcal{L}y,2}> &= \int_{\mathcal{X}_L} \rho \; d^2x \int_{\mathcal{Y}_R \cap J^+(x)} \rho \; d^2y \; e^{-\rho V^{LR}_{\mathcal{L}y}(x,y)} \\ &= \rho^2 \int_a^b dv_y \int_0^a du_y \int_0^{u_y} du_x \int_{-\infty}^0 dv_x \; e^{-\rho(u_x v_x + u_y v_y - a v_x)}. \end{aligned} \tag{5.14}$$

Note the upper limit of the u_x integral is now u_y, which is required to ensure $y \in J^+(x)$. This was automatically satisfied in all previous cases.

Solving the integrals one by one gives

$$<N^{LR}_{\mathcal{L}y,2}> = \rho \int_a^b dv_y \int_0^a du_y \int_0^{u_y} du_x \; \frac{e^{-\rho u_y v_y}}{a - u_x} \tag{5.15}$$

$$= -\rho \int_a^b dv_y \int_0^a du_y \; e^{-\rho u_y v_y} \ln\left(1 - \frac{u_y}{a}\right) \tag{5.16}$$

$$= -\int_a^b dv_y \; \frac{e^{-\rho a v_y}}{v_y}\left[\gamma + \ln(-\rho a v_y) + \Gamma(0, -\rho a v_y)\right], \tag{5.17}$$

where $\Gamma(s, x)$ is the incomplete gamma function [70]. It is generally true that

$$\Gamma(0, x) = -\gamma - \ln x - \sum_{k=1}^{\infty} \frac{(-x)^k}{k k!}, \tag{5.18}$$

and

$$\mathrm{Ei}(x) = \gamma + \ln|x| + \sum_{k=1}^{\infty} \frac{x^k}{k k!}, \qquad x \neq 0. \tag{5.19}$$

Therefore,

$$\begin{aligned} \Gamma(0, -x) &= -\gamma - \ln(-x) - \sum_{k=1}^{\infty} \frac{x^k}{k k!} \\ \ln(-x) + \Gamma(0, -x) &= -\gamma - \sum_{k=1}^{\infty} \frac{x^k}{k k!} \\ &= -\mathrm{Ei}(x) + \ln|x|. \end{aligned} \tag{5.20}$$

In the macroscopic regime, $\mathrm{Ei}(\rho a v_y) \gg \ln|\rho a v_y| > \gamma$. Thus by substituting into equation (5.17) and dropping non-leading terms,

$$<N^{LR}_{\mathcal{L}y,2}> \simeq \int_a^b dv_y \; \frac{e^{-\rho a v_y}}{v_y} \mathrm{Ei}(\rho a v_y). \tag{5.21}$$

Finally, using the asymptotic expansion for $\mathrm{Ei}(x)$, equation (5.2), one obtains

$$\begin{aligned} <N^{LR}_{\mathcal{L}y,2}> &\simeq \int_a^b dv_y \; \frac{1}{v_y}\left[\frac{1}{\rho a v_y} + \mathcal{O}\left(\frac{1}{(\rho a v_y)^2}\right)\right] \\ &= \frac{1}{\rho a^2} - \frac{1}{\rho a b} + \mathcal{O}\left(\frac{1}{(\rho a^2)^2}\right) - \mathcal{O}\left(\frac{1}{(\rho a b)^2}\right) \\ &\simeq \frac{1}{\rho a^2}, \end{aligned} \tag{5.22}$$

to leading order. This tends to 0 in the macroscopic regime as required for locality. Note that no other non-local contribution gives higher order corrections to the right-right contribution.

5.3 Final Result and Discussion

By combining the right-right contribution for y-links, equation (5.11), with the discussion and results regarding the non-local corrections with $x \overline{\in} \mathcal{X}$, equation (5.22), the total expected number of y-links in $2d$ is given by

$$<N_{\mathcal{L}y,2}> = 2 <N^{RR}_{\mathcal{L}y,2}> + <N^{LR}_{\mathcal{L}y,2}> + \ldots \tag{5.23}$$

$$= \frac{\pi^2}{3} - 2\,\mathrm{Li}_2\left(\frac{a}{b}\right) + \mathcal{O}\left(\frac{1}{\rho a^2}\right) \tag{5.24}$$

$$= \frac{\pi^2}{3} - \mathcal{O}\left(\frac{a}{b}\right) + \mathcal{O}\left(\frac{1}{\rho a^2}\right), \tag{5.25}$$

to leading order in corrections. This is both local and satisfies equation (4.8) with $k_2 = \pi^2/6$.

Using the approximate $\mathcal{X} \leftrightarrow \mathcal{Y}$ symmetry from section 4.2.4, one can define an approximately equivalent link, an x-link, which has constraints $x \overline{\in} J^-(\Sigma)$ and $y \underline{\in} \mathcal{Y}$. This new link corresponds to reflecting the empty volume $V_{\mathcal{L}y}(x, y)$ in the mirror symmetry axis associated with the $\mathcal{X} \leftrightarrow \mathcal{Y}$ symmetry. To see this compare figure 5.4 with figure 5.2. The same leading order result in the macroscopic regime as for y-links is expected by symmetry [15]. Thus there are two types of link that are viable horizon molecules in $1 + 1D$.

Finally, one can define an xy-link, such that $x \overline{\in} J^-(\Sigma)$ and $y \underline{\in} J^+(H)$. This the strictest type of link considered as it has the largest empty volume, as seen in figure 5.4. Therefore it should satisfy the locality conditions, but have a less than or equal k_2 value than above. It also is naturally symmetric, as it constrains x and y to equal extents, which is an appealing feature. However, we were unable to count these links analytically and thus applied computational techniques.

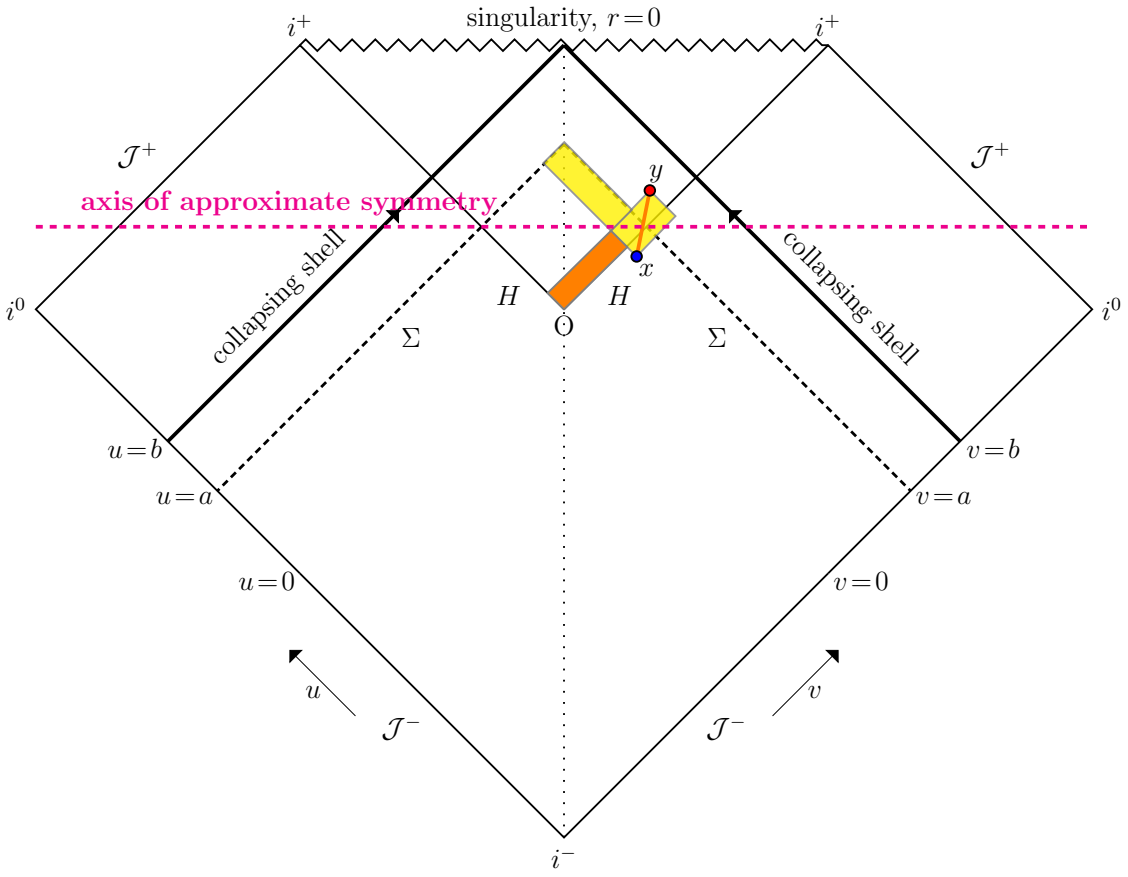

Figure 5.4: Penrose diagram (figure 4.3) showing the empty volume of an x-link (yellow) and xy-link (yellow and orange).

Chapter 6

Computationally Counting Links

This chapter presents a general n-dimensional algorithm for computationally counting links. This is then implemented in Python to count links in $2d$ and $3d$.

6.1 Computationally Finding All Minimal/Maximal Points

First consider an algorithm for finding all the minimal or maximal elements of a causet C faithfully embedded in a spacetime region R. Let Y be the list of the coordinates of each sprinkled point y_i^μ, written as y_i for shorthand. Note y_i^0 is the time coordinate of y_i.

First, an algorithm for finding the minimal elements:

1. **Sort the elements of Y into an ascending time ordered list, Y_T.** $Y_T = \{y_0, y_1, y_2, ...\}$, where $y_i^0 < y_{i+1}^0 \ \forall i$.

2. **Append y_0 to a list of points minimal in R, Y_{min}.** No y_i has a smaller time coordinate than y_0, therefore y_0 minimal.

3. **Find all points in $J^+(y_0)$ and remove them, together with y_0, from Y_T.** All points in $J^+(y_0)$ cannot be minimal in R as each point contains y_0 in its past. Also, all points in $J^+(y_0)$ are not in the causal past of any of the remaining points. Hence they may be removed from consideration. Practically, this was implemented using the ufunc `numpy.where` [71] to find all sprinkled points satisfying the condition $y_i^0 - y_0^0 > \sqrt{\sum_{k=1}^{n-1}(y_i^k - y_0^k)^2}$. `numpy.where` was used instead of an explicit `for` loop iteration over the sprinkled points as it is considerably more efficient.

4. **If Y_T is not empty, go to step 2. Else, stop.** The first element in the truncated Y_T (the new y_0) has the lowest time coordinate of all remaining points.

This produces a list of the minimal points in R, Y_{min}. An analogous algorithm can find all maximal points in R, the only differences are that a descending time order is applied and $J^-(y_0)$ is discarded at each iteration. Moreover, this algorithm is substantially faster than directly checking the minimality/maximality of every point because, after the time ordering, numerous points are discarded at each iteration with no extra computation.

6.2 Computational Method

Unlike in analytical calculations where an integral was found for the expected number of links, the code performs a sprinkling and directly counts links crossing the horizon. It then averages over N_{sp} sprinklings.

Four local link types of the form $x \overline{\in} A$ and $y \underline{\in} B$ arise from the discussion in chapter 5:

- $\mathcal{L}$: $x \overline{\in} \mathcal{X}$ and $y \underline{\in} \mathcal{Y}$
- $\mathcal{L}y$: $x \overline{\in} \mathcal{X}$ and $y \underline{\in} J^+(H)$
- $\mathcal{L}x$: $x \overline{\in} J^-(\Sigma)$ and $y \underline{\in} \mathcal{Y}$
- $\mathcal{L}xy$: $x \overline{\in} J^-(\Sigma)$ and $y \underline{\in} J^+(H)$

where $x \in \mathcal{X}$ and $y \in \mathcal{Y}$ in all cases. A general algorithm for counting any of these links is:

1. **Specify the type of link to be counted.**
2. **Input the numerical parameters**: a, b, ρ and N_{sp}.
3. **Define the spacetime region R to be sprinkled on.** See next section for example.
4. **Calculate the number of sprinkled points N, where N is taken from a Poisson distribution of mean ρV.** This was implemented using the `numpy.random` library.
5. **Uniformly distribute N points in R.** This completes the sprinkling process.
6. **Create arrays of all points within A and B.** This, again, was implemented using the equations of the boundaries of these regions with `numpy.where` to find all sprinkled points within the boundaries.
7. **Find all points maximal in A, A_{max}, and all points minimal in B, B_{min}.** See algorithm in previous section.
8. **If counting a link type for which $A \neq \mathcal{X}$: find all points in $\mathcal{X}$, then define $X_{max} := A_{max} \cap \mathcal{X}$. Else $X_{max} := A_{max}$.** This is needed to ensure $x \in \mathcal{X}$.
9. **If counting a link type for which $B \neq \mathcal{Y}$: find all points in $\mathcal{Y}$, then define $Y_{min} := B_{min} \cap \mathcal{Y}$. Else $Y_{min} := B_{min}$.** This is needed to ensure $y \in \mathcal{Y}$.
10. **Find all links between points in X_{max} and Y_{min}. Produce an array of all linked x-y pairs and count the number of links.** To do this, the sprinkled points in $J^+(x) \cap J^-(y)$ are found for each x-y pair. If there are no points in this region, and x and y are causally related, then x-y is a link.
11. **Repeat steps 4-10 N_{sp} times. Save the number of links found in each iteration.**
12. **Compute the average number of links over all of the sprinklings (iterations). Compute the standard error in the mean.**
13. **Repeat steps 2-12 for different values of the numerical parameters to plot the variation of the average number of links.** For example a and ρ could be held fixed whilst varying b in order to produce a plot of the average number of links against b.

Note, steps 8 and 9 above can be amended to count any contribution. For example, for $<N^{LR}_{\mathcal{L}y}>$, replace $\mathcal{X} \to \mathcal{X}_L$ in step 8 and $\mathcal{Y} \to \mathcal{Y}_R$ in step 9.

6.3 Inaccuracy Due to Numerical Cutoff

Figure 6.1 shows a $1+1D$ example of the above algorithm with a $2L \times 2L$ square for the sprinkling region, where $L = \sqrt{2}b$ and the square is centred at O. Whilst this sprinkling region covers the entirety of $\mathcal{Y}$, it does not cover the entirety of $\mathcal{X}$, as $\mathcal{X}$ is infinite in size. Thus there is a numerical cutoff on $\mathcal{X}$, which varies with b because $L \sim b$. Therefore, increasing b both increases the size of $\mathcal{Y}$, as it should, but also increases the size of $\mathcal{X}$ considered by the simulation, which is a source of inaccuracy. If links are local this will have negligible effect in the macroscopic regime, however, for small b, numerical results should be less than analytical results. This numerical truncation of $\mathcal{X}$ will occur regardless of the sprinkling region, as $\mathcal{X}$ is infinitely large.

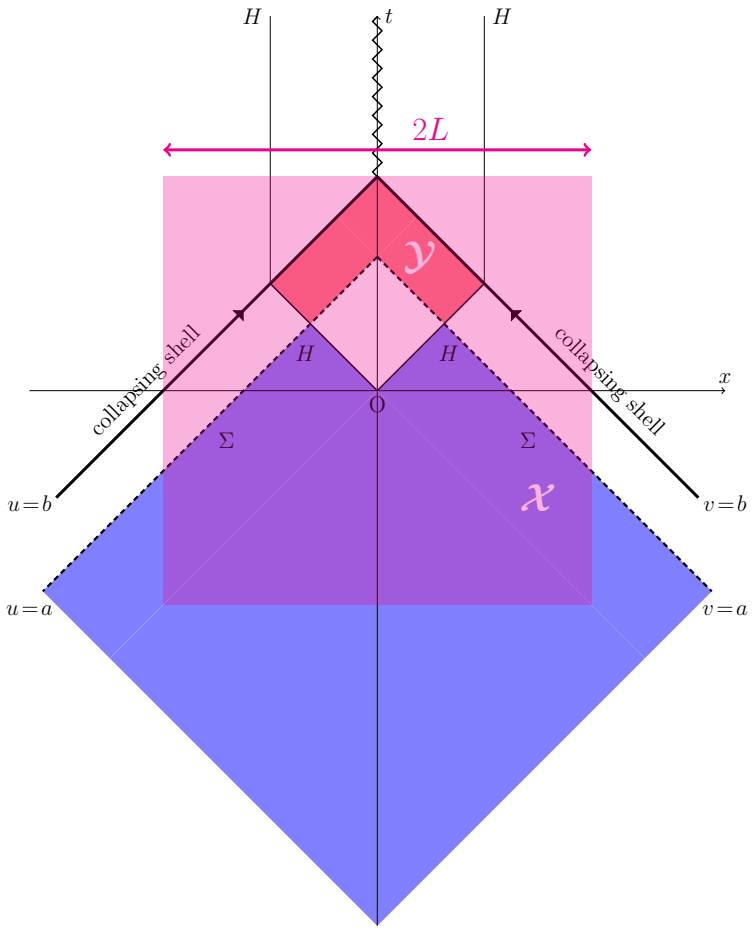

Figure 6.1: Numerical cutoff illustrated on a spacetime diagram (figure 4.1). The magenta square is an example of a region sprinkled on in the simulation and can be seen to fully encompass $\mathcal{Y}$ but not $\mathcal{X}$.

6.4 Test on Previous 1+1D Results

To test the algorithm, the code was setup to calculate the analytical results detailed in the previous chapter. In all cases, $N_{sp} = 1000$.

Firstly the code was made to study $<N_{\mathcal{L},2}^{RR}>$ as a function of b. This was calculated in section 5.1 and was found to be dependent on b according to equation (5.4). The plot in figure 6.2 shows the numerical data, for $\rho = 1$ and $a = 20$, overlaid with equation (5.4). There is good agreement between the data and the analytical result. Note, for low b the data is lower than the analytical result because of the numerical truncation of $\mathcal{X}$.

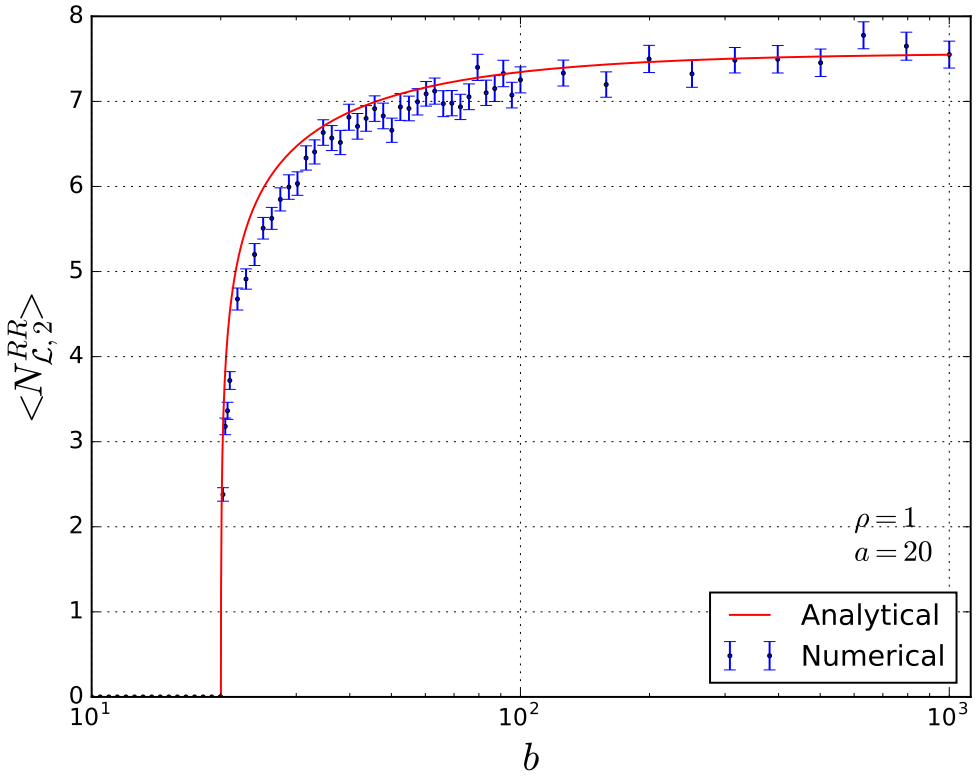

Figure 6.2: Numerical and analytical variation of $<N^{RR}_{\mathcal{L},2}>$ with b. Less data points are used for high b because the time of computation is longer as there are more points to consider.

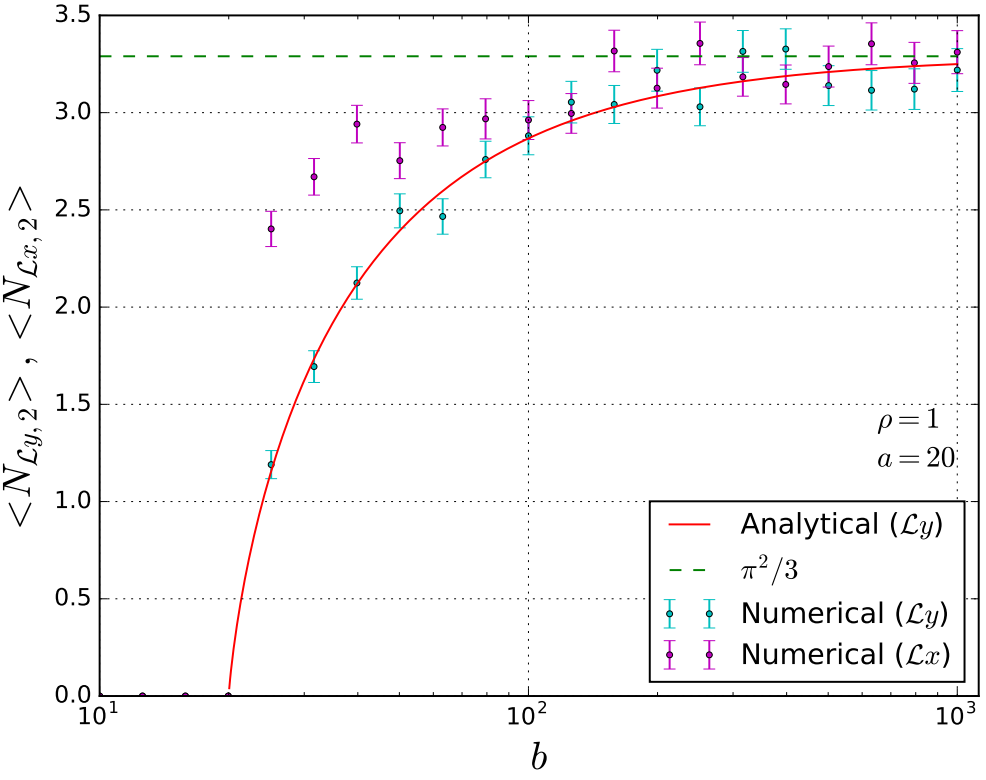

Figure 6.3: Variation of $<N_{\mathcal{L}y,2}>$ (numerical and analytical) and $<N_{\mathcal{L}x,2}>$ (numerical) with b. Note the agreement in the macroscopic regime, but discrepancy of x-links elsewhere.

Figure 6.3 shows the computational data for $<N_{\mathcal{L}y,2}>$ and $<N_{\mathcal{L}x,2}>$. It can be seen that $<N_{\mathcal{L}y,2}>$ agrees with the analytical result for y-links, equation (5.25), suggesting the non-local contributions are negligible as argued in section 5.2. Moreover, whilst $<N_{\mathcal{L}x,2}>$ is not equal to $<N_{\mathcal{L}y,2}>$ for low b, the two are compatible in the macroscopic regime, as expected by $\mathcal{X} \leftrightarrow \mathcal{Y}$ symmetry. The reason x-links reach $\pi^2/3$ faster than y-links is because, unlike $\mathcal{Y}$, $\mathcal{X}$ is not cutoff by the collapsing shell at lightcone coordinate b. Therefore, analytically, x-links should have a negligible b dependence, however the simulation results show some b dependence due to the numerical truncation of $\mathcal{X}$.

The agreement of the data with the corresponding analytical results in the macroscopic limit support the code's accuracy and its ability to efficiently find $\mathcal{O}(1)$ suitably constrained links out of up to $N \sim \rho V \sim \rho b^2 = 10^6$ sprinkled points (i.e. 10^{36} potential pairings).

6.5 Counting xy-links in $1+1D$

Figure 6.4 shows the variation of $<N^{RR}_{\mathcal{L}xy,2}>$ with ρ, which can be seen to tend to 0 in the macroscopic regime. This gives $k_2 = 0$, therefore xy-links cannot be horizon molecules in $1+1D$.

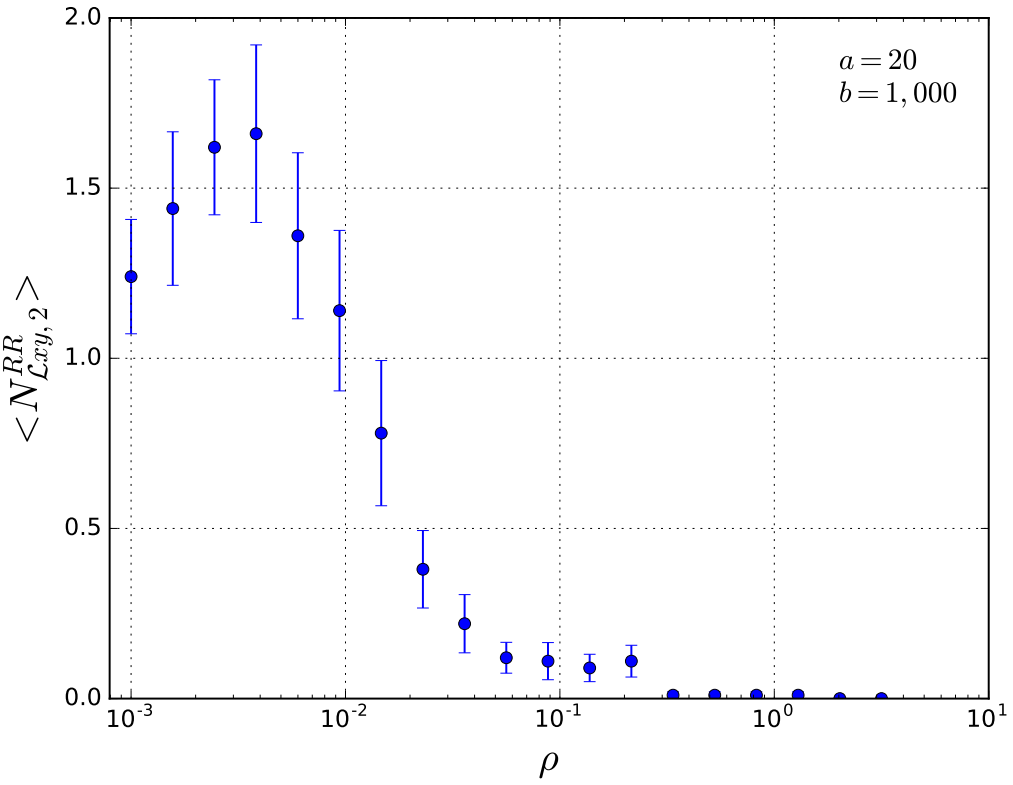

Figure 6.4: Numerical variation of $<N^{RR}_{\mathcal{L}xy,2}>$ with ρ.

6.6 Counting Links in $2+1D$

Analytical calculations in $2+1D$ are more complicated that in $1+1D$ because of the need to consider the volume of intersection of higher dimensional lightcones. Whilst success was made in calculating these volumes [14], using them within equation (3.5) appears analytically intractable. Thus a computational approach is adopted.

For the constant θ slice detailed in section 4.2.2, the cubic analogue of the square pictured in figure 6.1 was used for the sprinkling region. Because they are the most highly constrained, xy-links provide a lower bound for the expected number of all links considered above, thus they will be investigated first. Using equation (4.7), the expected number of xy-links must satisfy

$$<N_{\mathcal{L}xy,3}> \simeq k_3 \sqrt{2}\pi a \ \rho^{1/3}. \tag{6.1}$$

This is independent of b, therefore the software was used to plot $<N_{\mathcal{L}xy,3}>$ against b. Figure 6.5 shows this plot and it can be seen that, for $\rho = 0.01$ and $a = 20$, the average number of links is unbounded with b up to $b = 100$. For these parameters, $a/b = 0.2$ and $(\rho a^3)^{-1} = 0.01$, which are relatively small compared to the values of $<N_{\mathcal{L}xy,3}>$, suggesting this variation is not due to correction terms of similar form to those in equation (5.25).

This variation with b suggests that xy-links are non-local to $H \cap \Sigma$ in $2+1D$ and that they extend to the shell. This is apparent in figure 6.6 which shows a spacetime plot of the xy-links found in a sprinkling. Even with xy-links, where y is forced to be close to H and x is forced to be close to Σ, there are still links far away from $H \cap \Sigma$, with some reaching the shell. Moreover, many links extend outside both H and Σ. This can be understood using figure 6.7. Given any x maximal in $J^-(\Sigma)$, the locus of the intersection of $J^+(x)$ with H is a curve. Any y lying close to this curve will likely both link to x and be minimal in $J^+(H)$. Given the curve extends up to the shell, it is expected that xy-links can reach arbitrarily close to the shell [16]. Thus all links are rejected from being horizon molecules in $2+1D$. Also, given $3+1D$ can be thought of as a collection of $2+1D$ slices, it is expected the same is true in $3+1D$.

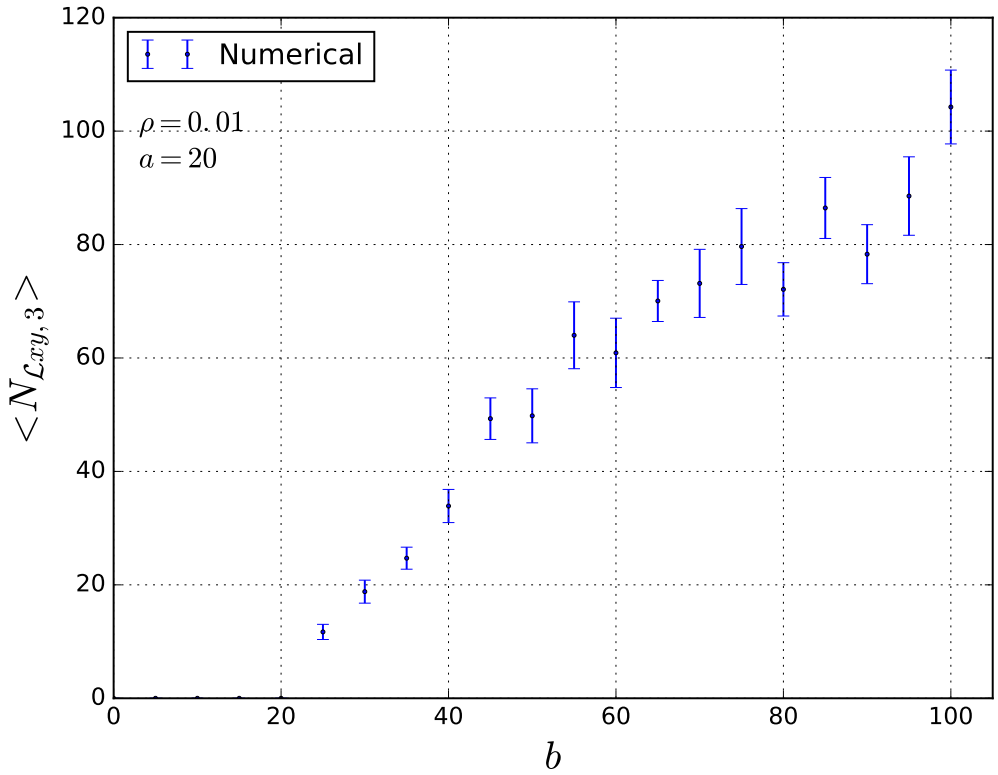

Figure 6.5: Numerical variation of $<N_{\mathcal{L}xy,3}>$ with b. $<N_{\mathcal{L}xy,3}>$ appears unbounded.

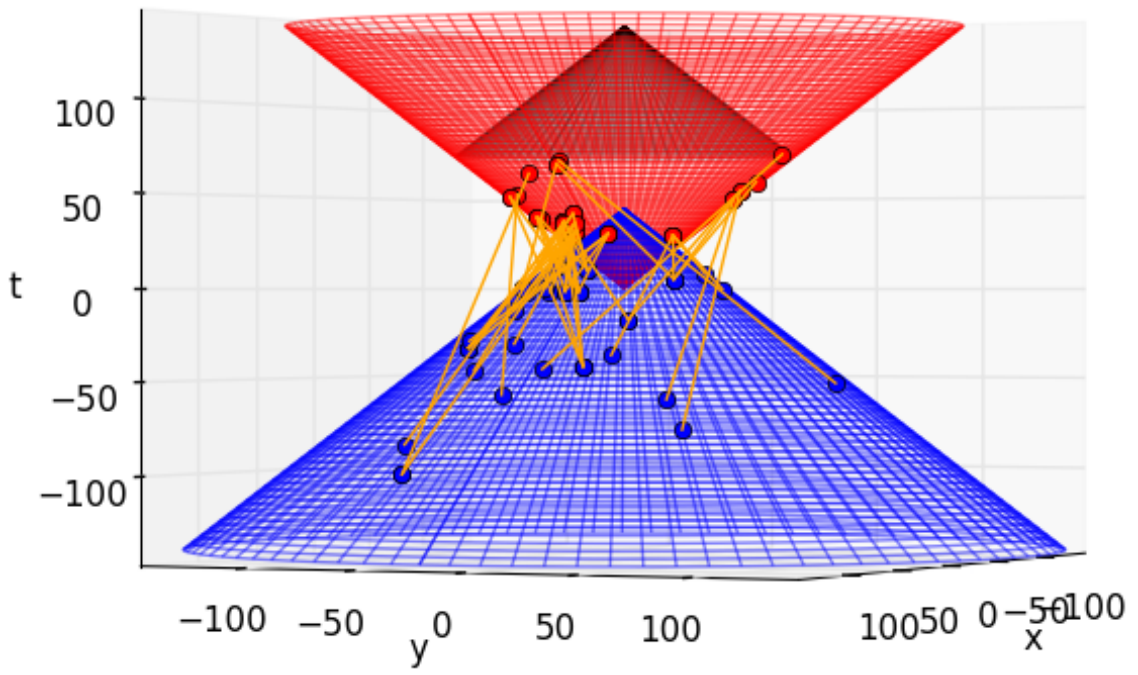

Figure 6.6: Simulation of links in $2+1D$. All links found by the simulation are plotted in orange with their corresponding two elements. The red cone represents H, the blue cone Σ, and the black cone represents the shell. It can be seen that links lie arbitrarily far away from $H \cap \Sigma$ (the intersection of the blue and red cones).

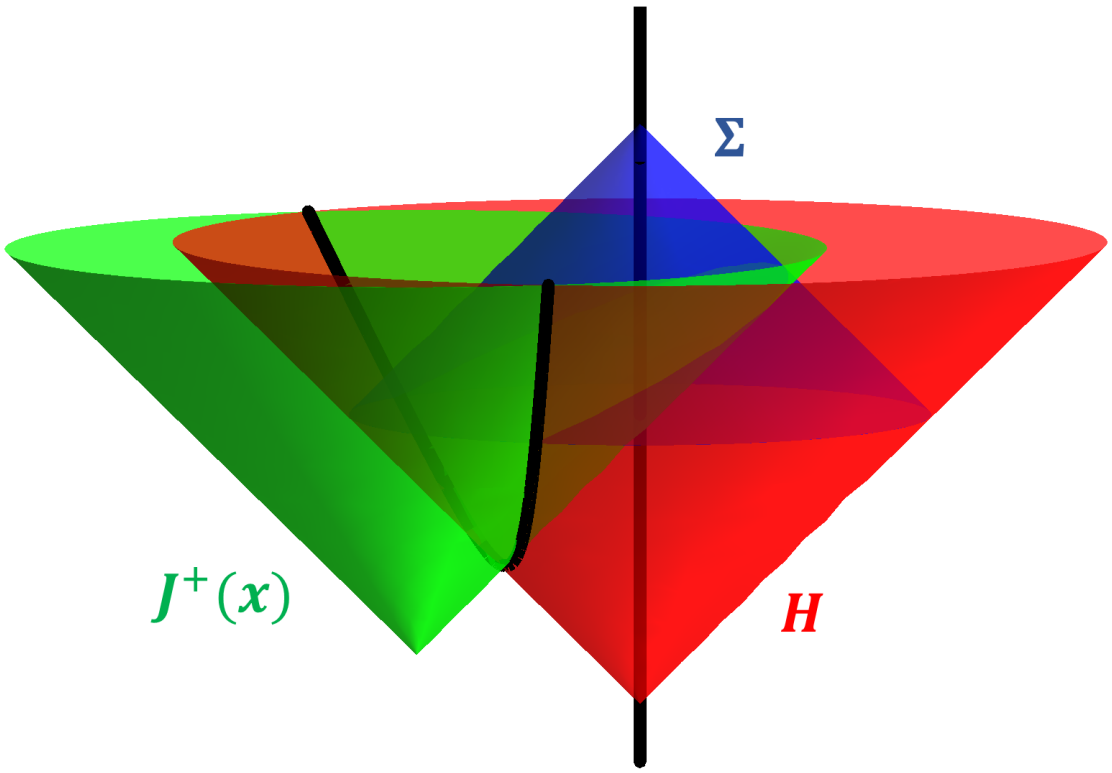

Figure 6.7: The red cone represents H, the blue cone Σ, and the green cone $J^+(x)$ for some arbitrary x. $J^+(x)$ and H intersect in a curve, shown in black. In order for y to link to x and be minimal in $J^+(H)$, it must be close to both $J^+(x)$ and H, i.e. close to $J^+(x) \cap H$. Because this intersection is a curve that will extend to the shell (not shown), each x has arbitrarily many y's linked to it lying arbitrarily far away from $H \cap \Sigma$. [72]

Chapter 7

Triplets

There are no other known minimal/maximal constraints capable localising links in $2+1D$. Therefore, a natural next step for finding a local molecule is to add an additional element to a link, forming a *triplet*.

7.1 Analytically Counting z-triplets in $1+1D$

There are various ways of adding an element to a link within the vicinity of $H \cap \Sigma$. One promising type of triplet introduced by Marr is known as a z-triplet [16], pictured in figure 7.1. It is defined such that, as well as $x \in \mathcal{X}$ and $y \in \mathcal{Y}$, there is a point $z \in J^+(H) \cap J^-(\Sigma)$, where $x \prec\!* \; z \prec\!* \; y$. To satisfy both of these conditions it is required that $z \in \mathcal{Z} := J^+(H) \cap J^-(\Sigma) \cap J^+(x) \cap J^-(y)$. Following Marr, we define the z-triplet with constraints $x \overline{\in} \mathcal{X}$ and $y \underline{\in} J^+(H)$, i.e. the same constraints as for a y-link.

Because y is linked to z, $y \in J^+(z)$, and because z is a random point in the sprinkling, this will have the indirect effect of increasing the empty volume since y is forced away from H. When constraining links earlier, a condition which directly increased the empty volume was imposed; adding a third atom indirectly has the same effect and therefore can be heuristically understood to increase the level of locality.

Using equation (3.5), recall the expected number of y-links is

$$<N_{\mathcal{L}y,n}> = \int_{\mathcal{X}} \rho \; d^n x \int_{\mathcal{Y} \cap J^+(x)} \rho \; d^n y \; e^{-\rho V_{\mathcal{L}y}(x,y)}, \tag{7.1}$$

where $V_{\mathcal{L}y}(x,y)$ is a volume containing no sprinkled points. In the case of a z-triplets, $V_{\mathcal{L}y}(x,y)$ must contain only one point, $z \in \mathcal{Z}$. Therefore to find the expected number of z-triplets $<N_{z,n}>$, a factor of $\rho d^n z$ must be added to the integrand, together with an integral over $\mathcal{Z}$. So,

$$<N_{z,n}> = \int_{\mathcal{X}} \rho \; d^n x \int_{\mathcal{Y} \cap J^+(x)} \rho \; d^n y \int_{\mathcal{Z}} \rho \; d^n z \; e^{-\rho V_{\mathcal{L}y}(x,y)}, \tag{7.2}$$

where the integrand is now the probability that $V_{\mathcal{L}y}(x,y)$ is empty apart from one point in $\mathcal{Z}$. Note $\mathcal{Z}$ is a function of x and y.

Because $V_{\mathcal{L}y}(x,y)$ is independent of z, as z lies within it but has no effect on its shape, integrating over $\mathcal{Z}$ yields

$$<N_{z,n}> = \int_{\mathcal{X}} \rho \; d^n x \int_{\mathcal{Y} \cap J^+(x)} \rho \; d^n y \; \rho V_{\mathcal{Z}}(x,y) \; e^{-\rho V_{\mathcal{L}y}(x,y)}, \tag{7.3}$$

where $V_{\mathcal{Z}}(x,y)$ is the volume of region $\mathcal{Z}$. Note this can be rewritten as

$$
\begin{aligned}
<N_{z,n}> &= \int_{\mathcal{X}} \rho \; d^n x \int_{\mathcal{Y}\cap J^+(x)} \rho \; d^n y \; \rho V_{\mathcal{Z}} \; e^{-\rho V_{\mathcal{Z}}} \; e^{-\rho(V_{\mathcal{L}y}-V_{\mathcal{Z}})} \\
&= \int_{\mathcal{X}} \rho \; d^n x \int_{\mathcal{Y}\cap J^+(x)} \rho \; d^n y \;\; \mathrm{Po}[1;\rho V_{\mathcal{Z}}] \;\; \mathrm{Po}[0;\rho(V_{\mathcal{L}y}-V_{\mathcal{Z}})],
\end{aligned}
\tag{7.4}
$$

showing that the integrand is the probability of there being one point in $V_{\mathcal{Z}}$ and none in the remaining volume $V_{\mathcal{L}y} - V_{\mathcal{Z}}$, as wanted.

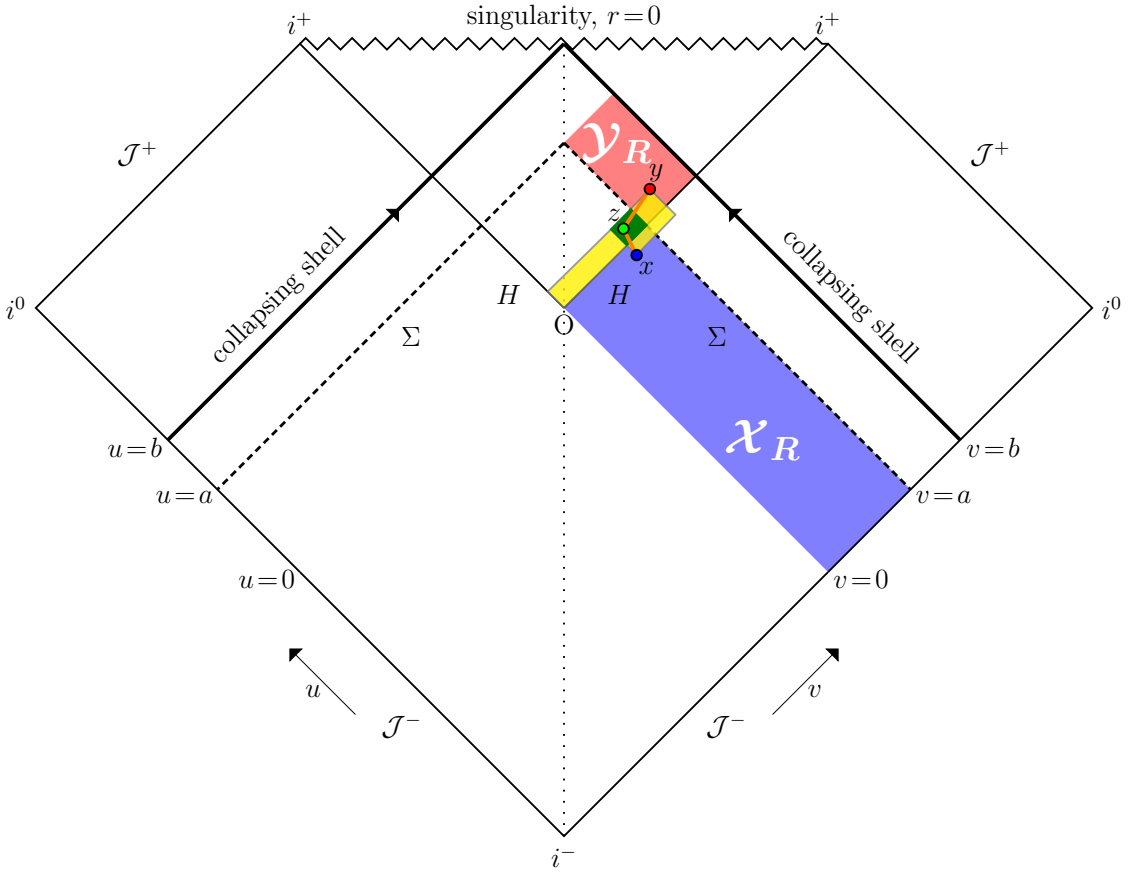

Figure 7.1: Penrose diagram (figure 4.4) depicting a z-triplet. The green point is z. The yellow region is the empty volume. The dark green region is $\mathcal{Z}$.

Because of their additional element, z-triplets are more constrained than y-links, thus regions that were found to negligibly contribute to y-links will also negligibly contribute here. Therefore there is no need to check the non-local contributions and it can be assumed that $<N_{z,2}> \simeq 2 < N^{RR}_{z,2}>$ to leading order, as in equation (4.11). Using equation (7.3), with equation (5.7) for $V_{\mathcal{L}y}$, one obtains

$$
\begin{aligned}
<N^{RR}_{z,2}> &= \rho^3 \int_{\mathcal{X}_R} d^2x \int_{\mathcal{Y}_R} d^2y \; V_{\mathcal{Z}} \; e^{-\rho V_{\mathcal{L}y}(x,y)} \\
&= \rho^3 \int_a^b dv_y \int_0^a du_y \int_0^a dv_x \int_{-\infty}^0 du_x \; (a-v_x)u_y \; e^{-\rho[u_x v_x + u_y v_y - u_x v_y]} \\
&= \rho^2 \int_a^b dv_y \int_0^a du_y \int_0^a dv_x \; \frac{(a-v_x)u_y}{v_y - v_x} \; e^{-\rho u_y v_y} \\
&= \rho^2 \int_a^b dv_y \int_0^a du_y \; \left[a - a\ln\left(1-\frac{a}{v_y}\right) + v_y \ln\left(1-\frac{a}{v_y}\right) \right] u_y e^{-\rho u_y v_y}
\end{aligned}
$$

$$= \int_a^b dv_y \; \frac{1}{v_y^2} \left[a - a \ln\left(1 - \frac{a}{v_y}\right) + v_y \ln\left(1 - \frac{a}{v_y}\right) \right] \left[1 - (1 + \rho a v_y) e^{-\rho a v_y} \right].$$

The second square brackets contains an exponentially small contribution in the macroscopic regime since $(1 + \rho a v_y) e^{-\rho a v_y} \ll 1$, which can be dropped to determine the leading order contribution. Thus,

$$\begin{aligned} <N_{z,2}^{RR}> &\simeq \int_a^b dv_y \; \frac{1}{v_y^2} \left[a - a \ln\left(1 - \frac{a}{v_y}\right) + v_y \ln\left(1 - \frac{a}{v_y}\right) \right] \\ &= a \int_a^b dv_y \; \frac{1}{v_y^2} - a \int_a^b dv_y \; \frac{1}{v_y^2} \ln\left(1 - \frac{a}{v_y}\right) + \int_a^b dv_y \; \frac{1}{v_y} \ln\left(1 - \frac{a}{v_y}\right) \\ &= \left[-\frac{a}{v_y} \right]_a^b - \left[\frac{a}{v_y} + \left(1 - \frac{a}{v_y}\right) \ln\left(1 - \frac{a}{v_y}\right) \right]_a^b + \left[\mathrm{Li}_2\left(\frac{a}{v_y}\right) \right]_a^b \\ &= - \left[2\frac{a}{v_y} + \left(1 - \frac{a}{v_y}\right) \ln\left(1 - \frac{a}{v_y}\right) \right]_a^b + \left[\mathrm{Li}_2\left(\frac{a}{v_y}\right) \right]_a^b . \end{aligned} \tag{7.5}$$

Using the fact

$$\lim_{x \to 1} \; (1 - x) \ln(1 - x) = 0,$$

the limits can be evaluated to give

$$\begin{aligned} <N_{z,2}^{RR}> &\simeq -2\frac{a}{b} - \left(1 - \frac{a}{b}\right) \ln\left(1 - \frac{a}{b}\right) + 2 + \mathrm{Li}_2\left(\frac{a}{b}\right) - \mathrm{Li}_2(1) \\ &= 2 - \frac{\pi^2}{6} - 2\frac{a}{b} - \left(1 - \frac{a}{b}\right) \ln\left(1 - \frac{a}{b}\right) + \mathrm{Li}_2\left(\frac{a}{b}\right). \end{aligned} \tag{7.6}$$

In order to find the order of the leading correction, use the series expansion for the logarithm and dilogarithm [69] as follows

$$\begin{aligned} <N_{z,2}^{RR}> &\simeq 2 - \frac{\pi^2}{6} - 2\frac{a}{b} + \left(1 - \frac{a}{b}\right) \sum_{n=1}^{\infty} \frac{1}{n} \left(\frac{a}{b}\right)^n + \sum_{n=1}^{\infty} \frac{1}{n^2} \left(\frac{a}{b}\right)^n \\ &= 2 - \frac{\pi^2}{6} - 2\frac{a}{b} + \sum_{n=1}^{\infty} \frac{1}{n} \left(\frac{a}{b}\right)^n - \sum_{n=1}^{\infty} \frac{1}{n} \left(\frac{a}{b}\right)^{n+1} + \sum_{n=1}^{\infty} \frac{1}{n^2} \left(\frac{a}{b}\right)^n \\ &= 2 - \frac{\pi^2}{6} - 2\frac{a}{b} + \frac{a}{b} + \sum_{n=2}^{\infty} \frac{1}{n} \left(\frac{a}{b}\right)^n - \sum_{n=2}^{\infty} \frac{1}{n-1} \left(\frac{a}{b}\right)^n + \frac{a}{b} + \sum_{n=2}^{\infty} \frac{1}{n^2} \left(\frac{a}{b}\right)^n \\ &= 2 - \frac{\pi^2}{6} + \sum_{n=2}^{\infty} \left[\frac{1}{n} - \frac{1}{n-1} + \frac{1}{n^2} \right] \left(\frac{a}{b}\right)^n \\ &= 2 - \frac{\pi^2}{6} - \sum_{n=2}^{\infty} \frac{1}{n^2(n-1)} \left(\frac{a}{b}\right)^n \\ &= 2 - \frac{\pi^2}{6} - \mathcal{O}\left(\left(\frac{a}{b}\right)^2 \right) \\ <N_{Z,2}> &\simeq 4 - \frac{\pi^2}{3} - \mathcal{O}\left(\left(\frac{a}{b}\right)^2 \right). \end{aligned} \tag{7.7}$$

This is lower than the value found for links, equation (5.25), as expected as the z-triplet is more constrained. Moreover, the leading order correction is quadratic in a/b, unlike for links where

it is linear, suggesting a higher level of locality. The result is of order unity and satisfies the condition of equation (4.8) with $k_2 = 2-\pi^2/6$. Note this result agrees with [16]. Note also there are expected to be correction terms that depend on a, b and ρ due to non-local contributions.

7.2 Computationally Counting z-triplets

A computational algorithm was employed to calculate the expected number of z-triplets in $2+1D$.

7.2.1 Computational Method

The first steps are identical to steps 1-5 in the link counting algorithm in section 6.2. From step 6 onwards the algorithm for z-triplets is as follows:

6. **Find all sprinkled points that are minimal in $\mathcal{Y}$. Append them to Y_{min}.**
7. **For every $y \in Y_{min}$ count the number of points in $J^+(H) \cap J^-(\Sigma) \cap J^-(y)$. If there is only one point, add it to Z and add y to Y, else discard that y.** This gives a list of z-y pairs where $z \prec\!* \; y$ and $z \in \mathcal{Z}$.
8. **For each (y, z) pair in Y and Z respectively, find all the points maximal in $J^-(z) \cap \mathcal{X}$.** These points are the points x, such that $x \prec\!* \; z$. Make a list of all (y, z, x) triplets.
9. **Check $J^+(x) \cap J^-(y) \cap J^-(H) \cap J^+(\Sigma)$ is empty for each triplet. If it is, append the triplet to a list of z-triplets and count them.** The final requirement to be satisfied is that, apart from z, $J^+(x) \cap J^-(y)$ is empty. However, there is no need to check the entirety of $J^+(x) \cap J^-(y)$ as the previous steps ensure emptiness elsewhere and it is computationally faster to search a smaller region of spacetime.
10. **Apply the z-triplet analogue of steps 11-13 for links.**

This algorithm uses the fact that if two points are linked, e.g. $x \prec\!* \; z$, then x is maximal in $J^-(z)$. Finding maximal/minimal points is substantially faster than checking if the causal interval, or some other region of spacetime, for each pair of points is empty. In fact, step 9 is the bottleneck of this algorithm, therefore minimality/maximality considerations are employed beforehand to reduce the number of points considered in this step.

7.2.2 $1+1D$ Test

Figure 7.2 shows a plot of $<N_{z,2}>$ against b using the square sprinkling region pictured in figure 6.1 with $\rho = 1$, $a = 10$ and $N_{sp} = 1000$. It is overlaid with the analytical result for $<N_{z,2}>$, using $<N_{z,2}> \simeq 2 <N_{z,2}^{RR}>$ (as z-triplets are local) and equation (7.6) for the right-right contribution. There is good agreement between the numerical and analytical results, providing support for the algorithm's accuracy.

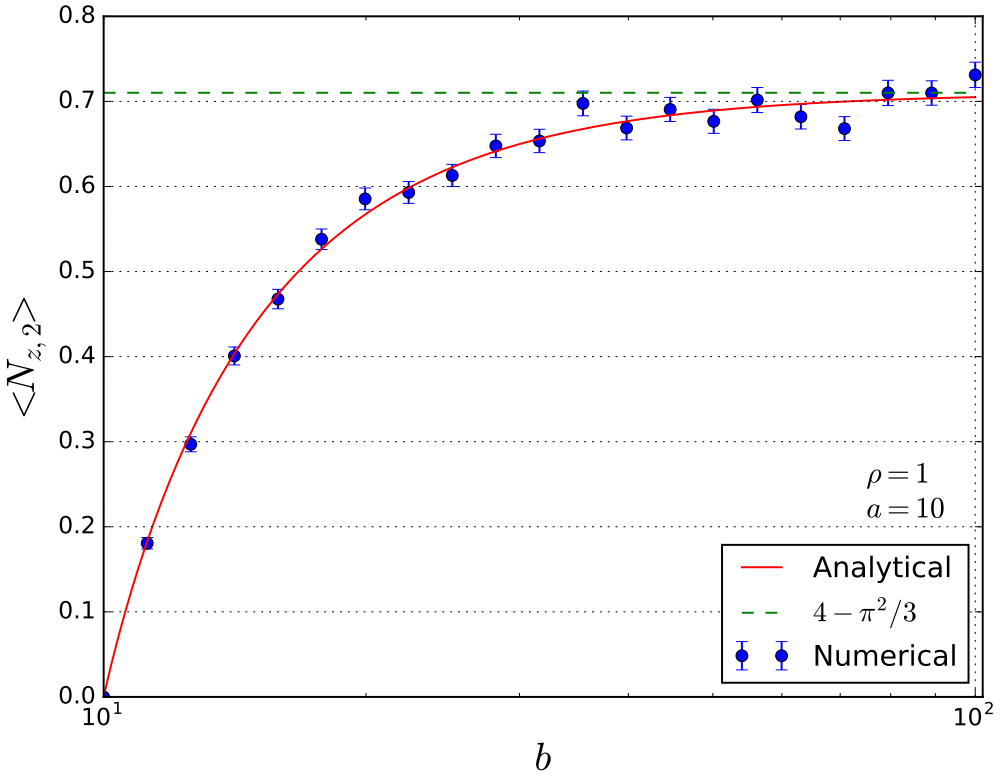

Figure 7.2: Numerical and analytical variation of $<N_{z,2}>$ with b.

7.2.3 $2+1D$ Results

Equation (4.7) requires

$$<N_{z,3}> = k_3 \sqrt{2}\pi a \ \rho^{1/3} \tag{7.8}$$

to be satisfied in the macroscopic regime in order for z-triplets to be viable horizon molecules.

Using a cubic sprinkling region, as for links, the simulation was first run to vary ρ between 10^{-3} and 10^{-1} for $a = 20$ and $b = 150$, as in figure 7.3. The values of the parameters ensure correspondence to the macroscopic regime, however it is expected that there will be correction terms. N_{sp} was varied with ρ from 1000 to 100 in order to ensure reasonable computation time for larger sprinklings. In order to test the satisfaction of equation (7.8), the following fit was performed using a least squares method [73, 74]:

$$<N_{z,3}> (a, \rho; k_3, c) = k_3 \sqrt{2}\pi a \ \rho^{1/3} + c, \tag{7.9}$$

where a constant c is added to account for correction terms. The fit is shown in figure 7.3 and gives an estimate of $\hat{k_3^\rho} = 0.28 \pm 0.02$, which is of order unity as required. Note that $\hat{c} = 1.8 \pm 0.2$, suggesting there are correction terms, although, $\hat{c}/ <N_{z,3}> \sim \mathcal{O}(0.1)$ throughout the plot, which is relatively small. The reduced chi-squared is $\chi^2_\nu = 1.4$ (p-value=0.2), suggesting there is no reason to reject z-triplets as horizon molecules to a reasonable significance.

In actuality the corrections are expected to be functions of a, b and ρ. By dimensional analysis and comparison with $1+1D$ links, the leading order corrections are expected to be of order a/b and $1/\rho a^3$. To investigate these corrections, the simulation was made to run over a range of a from 20 to 70 and over the same range of ρ as above, producing a 2 dimensional dataset as pictured in figure 7.4. A more general fit of

$$<N_{z,3}> (a, \rho; k_3, n, c, d) = k_3 \sqrt{2}\pi a \ \rho^n + c\frac{a}{b} + d\frac{1}{\rho a^3} \tag{7.10}$$

is used, which also takes the exponent of ρ as a free parameter n. This dataset yields $\hat{n} = 0.28 \pm 0.05$, which agrees with $1/3$ within error, as required. Also this gives an estimate of $\hat{k}_3 = 0.26 \pm 0.02$, which is consistent with $\hat{k}_3^{\rho}$. However, the reduced chi-squared is $\chi^2_\nu = 4.14$, which for the 62 degrees of freedom in this fit gives an extremely small p-value, suggesting a poor fit. This is likely due to the addition of extra parameters and guessing correction terms based on $1 + 1D$ links.

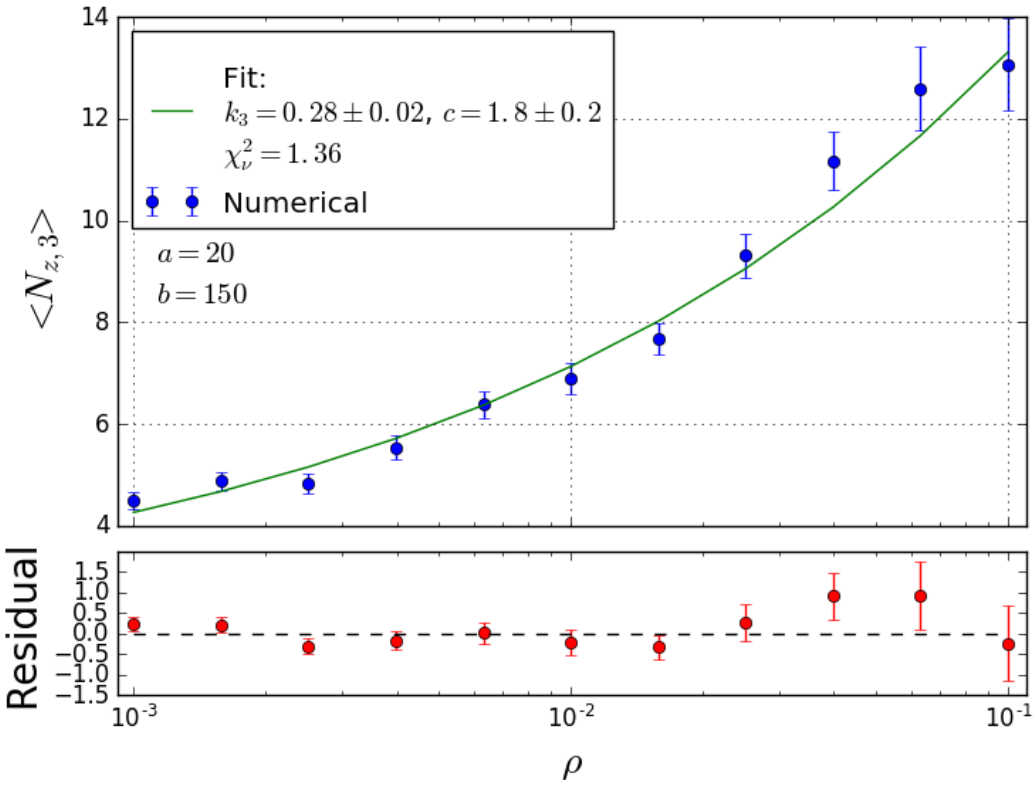

Figure 7.3: Numerical variation of $<N_{z,3}>$ with ρ. Equation (7.9) is fitted. Note the larger errors at larger ρ, because lower N_{sp} was used, increasing the standard error in the mean.

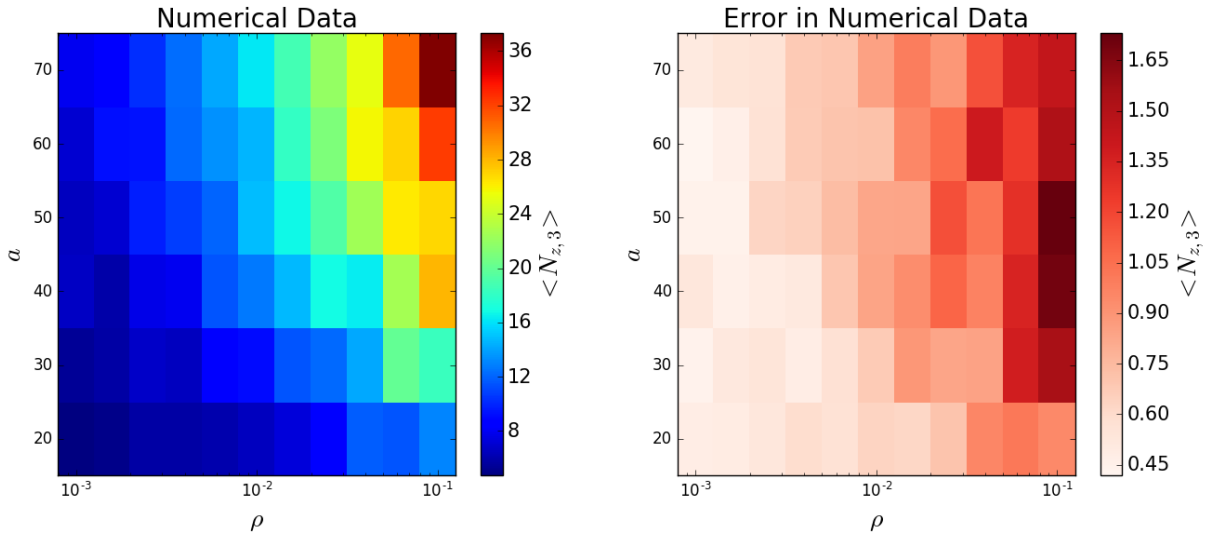

Figure 7.4: Numerical variation of $<N_{z,3}>$ with ρ and a, for $b = 150$.

To investigate the locality of z-triplets, consider figure 7.5, where it can be seen that they are local to $H \cap \Sigma$ as they do not extend arbitrarily far along H or Σ. Furthermore, the links

between x, z and y no longer cross from cone to cone without crossing $H \cap \Sigma$, as they did for links in figure 6.6. This is because z is required to lie in the future of H and the past of Σ, i.e. in the region enclosed by both the blue and red cones, as well as being linked to x and y. These conditions enforce x and y to be causally connected via a point inside both the H and Σ cones, thus making the z-triplet local to $H \cap \Sigma$. Altogether, these results show that z-triplets are viable horizon molecules.

Finally, although equation (2.8) is strictly for $4d$, one can heuristically consider the $3d$ analogue by changing the exponent on the left-hand side from 2 to 1 (as areas l^2 become lengths l). Therefore, assuming the factor of S_{BH} is also $1/4$ in $3d$, the fundamental length scale can be estimated as follows

$$\begin{aligned}\hat{l}_f &\approx 4\hat{k}_3^{\rho} l_P \\ &= 4 \times (0.28 \pm 0.02) \times 1.616 \times 10^{-35}\text{m} \\ &= (1.8 \pm 0.1) \times 10^{-35}\text{m},\end{aligned}$$

where $\hat{k}_3^{\rho}$ is used as it arises from the better fit. This illustrates how the value of l_f can be determined from the proposal.

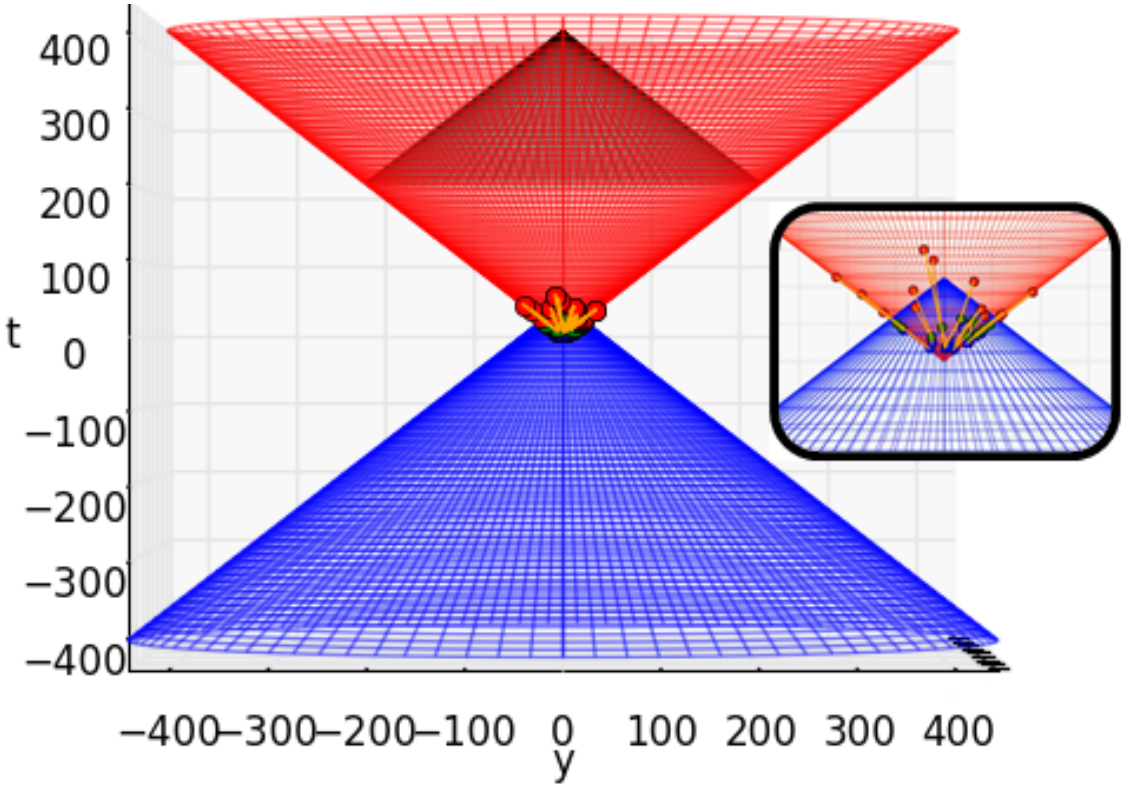

Figure 7.5: Plot of z-triplets found in a $2+1D$ sprinkling simulation (zoomed-in on right). Links are orange, x's are blue points, y's are red and z's green. The red cone represents H, the blue cone Σ, and the black cone represents the shell. It can be seen that z-triplets are local to $H \cap \Sigma$ (the intersection of the blue and red cones).

Chapter 8

Conclusion

This report has counted links and z-triplets in both $1+1D$ and $2+1D$. Having found plain links are non-local in $1+1D$, it was shown that by applying appropriate minimality/maximality constraints one can obtain local links. However, computational analysis of $2+1D$ showed that even the most constrained links (xy-links) are non-local, therefore ruling them out as horizon molecules. A second method of enforcing locality, adding a third atom to the molecule to create a z-triplet, was then discussed and shown to produce viable horizon molecules in both $1+1D$ and $2+1D$. The success of z-triplets provides promise for Sorkin's proposal moving forward.

In terms of future work, the code could be run on a better computer in order to consider larger causets, in turn extending further into the macroscopic regime and providing more accurate results. The largest number of sprinkled points that could be stored on the computer used in this work was of order 1 million, which limited the runs above. Larger causet simulations could also make $3+1D$ computations feasible.

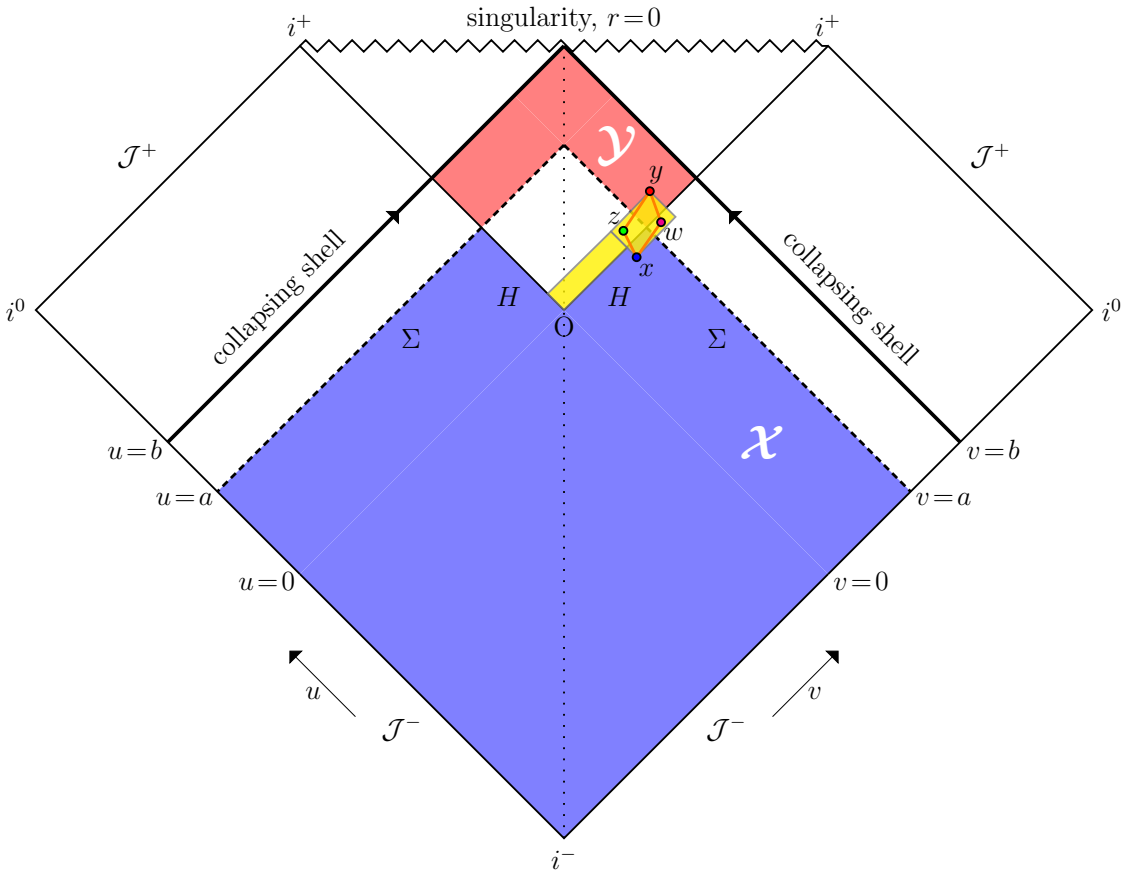

Figure 8.1: Penrose diagram (figure 4.3) illustrating a diamond molecule.

The code could also be adjusted to consider different types of z-triplet, with different minimality/maximality constraints on x and y. Moreover, different types of molecules could be investigated. One molecule of particular interest is the *diamond*, pictured in figure 8.1. This is a 4-atom molecule which looks like pair creation at x, with one atom moving into the horizon (z) and one staying outside (w), with a 'witness' at y observing the entanglement. This is akin to Hawking radiation [75], a seemingly alternative explanation for black hole entropy, however it is possible that diamond molecules are the quantum gravitational analogue of Hawking radiation. Diamonds have already been shown to satisfy the proposal analytically in $1+1D$ [76].

Finally, the computational method could be extended to study horizons in more complex geometries. In this work only the flat spacetime within a collapsing shell was considered, however one could also study other black holes, such as a static Schwarzschild black hole formed after the collapse, or a BTZ black hole [77], both of which seem analytically intractable.

The software developed in this work lays the framework for the study of many other molecules and spacetime geometries. This report has only scratched the surface of its potential capabilities.

Bibliography

[1] A. Einstein, Grundlage der allgemeinen Relativitätstheorie (The Foundation of the General Theory of Relativity), Annalen der Physik (ser. 4) **49** 769–822 (1916).

[2] E. F. Taylor, J. A. Wheeler, Exploring Black Holes: Introduction to General Relativity, Addison-Wesley, (2016). ISBN 0-201-38423-X

[3] J.D. Bekenstein, Black holes and entropy, Physical Review D. **7** 2333–2346 (1973). doi:10.1103/PhysRevD.7.2333.

[4] S.W. Hawking, Particle creation by black holes, Communications in Mathematical Physics. **43** 199–220 (1975). doi:10.1007/BF02345020.

[5] L. Bombelli, J. Lee, D. Meyer, and R. D. Sorkin, Space-time as a causal set, Phys. Rev. Lett. **59**, 521 (1987).

[6] R.D. Sorkin, in Lectures on Quantum Gravity, Proceedings of the Valdivia Summer School, edited by A. Gomberoff and D. Marolf (Plenum, New York, 2005). eprint: gr-qc/0309009

[7] R.D. Sorkin, Ten theses on black hole entropy (Perimeter Inst. Theor. Phys. & Syracuse U.), Stud.Hist.Phil.Sci. B**36** 291-301 (2005).

[8] W.G. Unruh, Experimental black hole evaporation, Phys. Rev. Lett. **46** 1351 (1981).

[9] C. Barceló, S. Liberati, M. Visser, Towards the observation of Hawking radiation in Bose–Einstein condensates, Int. J. Mod. Phys. A. **18** 3735–3745 (2003). arXiv:gr-qc/0110036. doi:10.1142/s0217751x0301615x.

[10] S. Das, Black hole thermodynamics: Entropy, information and beyond, Pramana **63** 797-816 (2004). DOI: 10.1007/BF02705201

[11] O. Lahav, A. Itah, A. Blumkin, C. Gordon & J. Steinhauer, A sonic black hole in a density-inverted Bose–Einstein condensate, Phys.Rev.Lett. **105** 240401 (2010) (2009). arXiv:0906.1337

[12] J. Steinhauer, Observation of self-amplifying Hawking radiation in an analogue black-hole laser, Nat Phys **10** 864 (2014) doi:10.1038/nphys3104.

[13] J. Steinhauer, Observation of quantum Hawking radiation and its entanglement in an analogue black hole, Nature Physics. **12** 959–965 (2003). doi:10.1038/nphys3863.

[14] D. Dou, Causal sets, a possible interpretation for the black hole entropy and related topics, (SISSA, Trieste) (1999) e-Print: gr-qc/0106024

[15] D. Dou, R.D. Sorkin, Black hole entropy as causal links, Found.Phys. **33** 279-296 (2003).

[16] S.K. Marr, Black hole entropy from causal sets (PhD Thesis), Imperial College London (2007).

[17] K. Schwarzschild, On the gravitational field of a mass point according to Einstein's theory, Sitzungsber.Preuss.Akad.Wiss.Berlin (Math. Phys.) 189-196 (1916).

[18] F. Dowker, Black Holes (Lecture Notes), Imperial College London (2014).

[19] C.W. Misner, K.S.Thorne, J. A. Wheeler, Gravitation, W.H. Freeman, (1970). ISBN 0-7167-0344-0.

[20] H. Reall, Part 3 Black Holes (Lecture Notes), University of Cambridge (2014).

[21] J. M. Bardeen, B. Carter, S. W. Hawking, The four laws of black hole mechanics, Communications in Mathematical Physics. **31** 161–170 (1973).

[22] E. Fermi, Thermodynamics, Dover Publications Inc.; New Ed (2000). ISBN-10: 048660361X

[23] J.D. Bekenstein, Black-hole thermodynamics, Physics Today **33** 24-31 (1980).

[24] D. Page, Hawking Radiation and Black Hole Thermodynamics, New Journal of Physics. **7** 203 (2004) arXiv:hep-th/0409024

[25] NIST, "Planck length", NIST's published CODATA constants `http://physics.nist.gov/cgi-bin/cuu/Value?plkl`

[26] R.D. Sorkin, Toward a Proof of Entropy Increase in the Presence of Quantum Black Holes, Phys Rev. Lett. **56**, 1885 (1986).

[27] P. Majumdar, Black hole entropy and quantum gravity, Indian J.Phys. B**73** 147 (1999). IMSC-98-07-38

[28] J.D. Bekenstein, Information in the Holographic Universe, Scientific American **17** 66-73 (2007).

[29] Zero Point, `http://www.zeropoint.ca/GSSD-4-7UniHologram.html` Accessed: 01/05/17.

[30] R.D. Sorkin, On the Entropy of the Vacuum Outside a Horizon, General Relativity and Gravitation, Vol. 1, Classical Relativity. Proceedings of the 10th International Conference on General Relativity and Gravitation, held July 4-9, 1983, in Padova, Italy. Edited by B. Bertotti, F. de Felice and A. Pascolini. Consiglio Nazionale delle Ricerche, Rome, 734 (1983).

[31] R.D. Sorkin, The statistical mechanics of black hole thermodynamics, Talk given at Conference: C96-12-14 (1997). e-Print: gr-qc/9705006

[32] J. Myrheim, CERN preprint TH-2538 (1978).

[33] G. 't Hooft, in Recent Developments in Gravitation (Proceedings of the 1978 Cargese Summer Institute), edited by M. Levy and S. Deser. Plenum, New York, (1979).

[34] F. Dowker, Causal sets as discrete spacetime, Contemp. Phys. **47**(1), 1–9 (2006).

[35] F. Dowker, Introduction to causal sets and their phenomenology, Gen. Relativ. Gravit. **45**(9), 1651–1667 (2013).

[36] R. Penrose: Techniques of Differential Topology in Relativity. SIAM, Philadelphia (1972).

[37] S.W. Hawking, A.R. King, P.J. McCarthy, A new topology for curved space–time which incorporates the causal, differential, and conformal structures, J. Math. Phys. **17**, 174 (1976).

[38] S.W. Hawking, G.F.R. Ellis, The Large Scale Structure of Space-Time. Cambridge University Press, Cambridge (1973).

[39] D.B. Malament, The class of continuous timelike curves determines the topology of spacetime, J. Math. Phys. **18**, 1399 (1977).

[40] A.V. Levichev, Prescribing the conformal eometry of a Lorentzian manifold by means of its causal structure, Soviet Math. Dokl. **35**, 452 (1987).

[41] O. Parrikar and S. Surya, Causal Topology in Future and Past Distinguishing Spacetimes, Class. Quantum Gravit. **28** (2011). doi:10.1088/0264-9381/28/15/155020

[42] J.L. Bell, The Continuous and the Infinitesimal in Mathematics and Philosophy, Polimetrica s.a.s., 145-148 (2005).

[43] R.D. Sorkin, "Geometry from order: causal sets" in: Einstein Online **2**, 1007 (2006).

[44] B. Dushnik and E.W. Miller, Partially Ordered Sets, Amer. J. Math. **63** 600-610 (1941).

[45] S.P. Johnston, Quantum Fields on Causal Sets, Imperial College London, (2010). e-Print: arXiv:1010.5514 [hep-th]

[46] J. Henson, The Causal set approach to quantum gravity, (2006). Published in D. Oriti (ed.): Approaches to quantum gravity, 393-413. e-Print: gr-qc/0601121

[47] L. Bombelli and D.A. Meyer, The origin of lorentzian geometry, Phys. Lett. **A141**, 226 (1989).

[48] L. Bombelli, Statistical Lorentzian geometry and the closeness of Lorentzian manifolds, J. Math. Phys. **41**, 6944-6958 (2000).

[49] J. Noldus, A Lorentzian Gromov-Hausdoff notion of distance, Class. Quant. Grav. **21** 839-850 (2004). e-print: gr-qc/0308074

[50] L. Bombelli and J. Noldus, The moduli space of isometry classes of globally hyperbolic spacetimes, Class. Quant. Grav. **21**, 4429 (2004). arXiv:gr-qc/0402049

[51] J. Henson, Constructing an interval of Minkowski space from a causal set, Class.Quant.Grav. **23** L29-L35 (2006). gr-qc/0601069

[52] D.P. Rideout and R.D. Sorkin, Evidence for a continuum limit in causal set dynamics, Phys. Rev. **D63**, 104011 (2001). gr-qc/0003117

[53] G. Brightwell and R. Gregory, Structure of random discrete spacetime, Phys. Rev. Lett. **66**, 260 (1991).

[54] R. Ilie, G.B. Thompson, and D.D. Reid, A numerical study of the correspondence between paths in a causal set and geodesics in the continuum, Class.Quant.Grav. **23** 3275-3286 (2006). gr-qc/0512073

[55] D. Rideout and P. Wallden, Spacelike distance from discrete causal order, Class. Quant. Grav. **26**, 155013 (2009). e-Print: arXiv:0810.1768 [gr-qc]

[56] R.D. Sorkin, Does locality fail at intermediate length-scales Towards Quantum Gravity ed (Cambridge: Cambridge University Press) (2007). arXiv:gr-qc/0703099

[57] D.M.T. Benincasa and F. Dowker, Scalar curvature of a causal set, Phys. Rev. Lett. **104** 181301 (2010). doi:10.1103/PhysRevLett.104

[58] F. Dowker and L. Glaser, Causal set d'Alembertians for various dimensions, Class. Quantum Grav. **30**, 195016 (2013).

[59] L. Glaser, A closed form expression for the causal set d'Alembertian, Classical and Quantum Gravity **31** 9 (2014).

[60] R. Gallager, Discrete Stochastic Processes, Massachusetts Institute of Technology: MIT OpenCourseWare, https://ocw.mit.edu. (2011) License: Creative Commons BY-NC-SA.

[61] G. Bohm and G. Zech, "Introduction to Statistics and Data Analysis for Physicists," Verlag Deutsches Elektronen-Synchrotron, (2010).

[62] B.F. Dribus, On the Axioms of Causal Set Theory, Louisiana State U., (2013). e-Print: arXiv:1311.2148 [gr-qc]

[63] L. Glaser, S. Surya, Towards a Definition of Locality in a Manifoldlike Causal Set, Phys.Rev. D**88** no.12 124026 (2013).

[64] D. Tong, Lectures on Statistical Physics, University of Cambridge (2011).

[65] E.W. Weisstein, "Hypersphere", MathWorld–A Wolfram Web Resource. `http://mathworld.wolfram.com/Hypersphere.html`

[66] E.W. Weisstein, "Exponential Integral", MathWorld–A Wolfram Web Resource. `http://mathworld.wolfram.com/ExponentialIntegral.html`

[67] E.W. Weisstein, "Euler-Mascheroni Constant", MathWorld–A Wolfram Web Resource. `http://mathworld.wolfram.com/Euler-MascheroniConstant.html`

[68] N. Bleistein, R.A. Handelsman, Asymptotic Expansions of Integrals, Dover (1986). ISBN 0-486-65082-0.

[69] E.W. Weisstein, "Dilogarithm", MathWorld–A Wolfram Web Resource. `http://mathworld.wolfram.com/Dilogarithm.html`

[70] E.W. Weisstein, "Incomplete Gamma Function" From MathWorld–A Wolfram Web Resource. `http://mathworld.wolfram.com/IncompleteGammaFunction.html`

[71] SciPy Reference Guide `https://docs.scipy.org/doc/numpy/reference/generated/numpy.where.html` Accessed: 01/05/17.

[72] B. Freivogela, M. Klebanc, A. Nicolisd and K. Sigurdsone, Eternal inflation, bubble collisions, and the disintegration of the persistence of memory Journal of Cosmology and Astroparticle Physics **2009** (2009).

[73] J. Wolberg, Data Analysis Using the Method of Least Squares: Extracting the Most Information from Experiments, Springer Science & Business Media (2006).

[74] SciPy Reference Guide `https://docs.scipy.org/doc/scipy/reference/generated/scipy.optimize.curve_fit.html` Accessed: 01/05/17.

[75] S.W. Hawkin, Black hole explosions?, Nature. **248**(5443) 30–31 (1974)

[76] C. Shuaib, The Statistical Mechanics and Thermodynamics of Black Holes (MSci Report), Imperial College London [currently unpublished] (2016).

[77] M. Bañados, C. Teitelboim, J. Zanelli, "The Black hole in three-dimensional space-time", Phys. Rev. Lett., American Physical Society, **69**(13) 1849–51 (1992).